ORNL/TM-2018/956
Revision 0

Safety Testing and Post-Safety-Test Examination of AGR-2 UCO Compact 2-3-2 and AGR-2 UO_2 Compact 3-4-1

John D. Hunn
Robert N. Morris
Fred C. Montgomery
Tyler J. Gerczak
Darren J. Skitt
Grant W. Helmreich
Brian D. Eckhart
Zachary M. Burns

September 2018

OAK RIDGE NATIONAL LABORATORY
MANAGED BY UT-BATTELLE FOR THE US DEPARTMENT OF ENERGY

ORNL/TM-2018/956

Fusion and Materials for Nuclear Systems Division

SAFETY TESTING AND POST-SAFETY-TEST EXAMINATION OF AGR-2 UCO COMPACT 2-3-2 AND AGR-2 UO_2 COMPACT 3-4-1

John D. Hunn
Robert N. Morris
Fred C. Montgomery
Tyler J. Gerczak
Darren J. Skitt
Grant W. Helmreich
Brian D. Eckhart
Zachary M. Burns

Revision 0

Date Published: September 2018

Work sponsored by
US DEPARTMENT OF ENERGY
Office of Nuclear Energy - Advanced Reactor Technologies
under the
Advanced Gas Reactor Fuel Development and Qualification Program

Prepared by
OAK RIDGE NATIONAL LABORATORY
Oak Ridge, TN 37831-6283
managed by
UT-BATTELLE, LLC
for the
US DEPARTMENT OF ENERGY
under contract DE-AC05-00OR22725

CONTENTS

REVISION LOG

Revision	Date	Affected Pages	Revision Description
0		All	Initial issue

LIST OF FIGURES

LIST OF TABLES

ACRONYMS

3D	Three-dimensional
AGR	Advanced Gas Reactor (Fuel Development and Qualification Program)
AGR-1	First AGR program irradiation experiment
AGR-2	Second AGR program irradiation experiment
BEC	Backscattered electron/scanning electron composite
BWXT	BWX Technologies
CCCTF	Core Conduction Cooldown Test Facility
CO	Carbon monoxide
DLBL	Deconsolidation leach-burn-leach
EDS	Energy-dispersive x-ray spectroscopy (EDS)
FACS	Fuel Accident Condition Simulator
FIMA	Fissions per initial metal atom
HTGR	High Temperature Gas-cooled Reactor
ID	Identification
IFEL	Irradiated Fuels Examination Laboratory (hot cells)
IMGA	Irradiated Microsphere Gamma Analyzer
INL	Idaho National Laboratory
IPyC	Inner pyrolytic carbon (TRISO layer)
M/C	Measured versus calculated (inventory fraction)
M/A	Measured versus average (inventory fraction)
OPyC	Outer pyrolytic carbon (TRISO layer)
ORNL	Oak Ridge National Laboratory
PIE	Post-irradiation examination
SEI	Scanning electron image
SEM	Scanning electron microscopy
SiC	Silicon carbide (TRISO layer)
TAVA	Time-averaged/volume-averaged temperature
TRISO	Tristructural-isotropic (coated particles)
UCO	Uranium carbide/uranium oxide mixture (fuel kernels)
UO_2	Uranium dioxide (fuel kernels)
Z	Atomic number

ACKNOWLEDGMENTS

This work was sponsored by the U.S. Department of Energy, Office of Nuclear Energy, through the Idaho National Laboratory Advanced Reactor Technologies Technology Development Office as part of the Advanced Gas Reactor Fuel Development and Qualification Program. Analysis of leach solutions and Core Conduction Cooldown Test Facility furnace components was provided by the Oak Ridge National Laboratory Nuclear Analytical Chemistry & Isotopics Laboratory. Hot cell activities were supported by the staff of the Oak Ridge National Laboratory Irradiated Fuels Examination Laboratory (IFEL).

1. INTRODUCTION AND BACKGROUND*

Post-irradiation examination (PIE) and elevated-temperature safety testing are being performed on tristructural-isotropic (TRISO) coated-particle fuel compacts from the Advanced Gas Reactor (AGR) Fuel Development and Qualification Program second irradiation experiment (AGR-2). Details on this irradiation experiment have been previously reported [Collin 2014]. The AGR-2 PIE effort builds upon the understanding acquired throughout the AGR-1 PIE campaign [Demkowicz et al. 2015] and is establishing a database for the different AGR-2 fuel designs.

The AGR-2 irradiation experiment included TRISO fuel particles coated at BWX Technologies (BWXT) with a 150-mm-diameter engineering-scale coater. Two coating batches were tested in the AGR-2 irradiation experiment. Batch 93085 had 508-µm-diameter uranium dioxide (UO_2) kernels. Batch 93073 had 427-µm-diameter UCO kernels, which is a kernel design where some of the uranium oxide is converted to uranium carbide during fabrication to provide a getter for oxygen liberated during fission and limit CO production. Fabrication and property data for the AGR-2 coating batches have been compiled [Barnes and Marshall 2009] and compared to AGR-1 [Phillips, Barnes, and Hunn 2010]. The AGR-2 TRISO coatings were most like the AGR-1 Variant 3 TRISO deposited in the 50-mm-diameter ORNL lab-scale coater [Hunn and Lowden 2006]. In both cases, the hydrogen and methyltrichlorosilane coating gas mixture employed to deposit the SiC was diluted with argon to produce a finer-grain, more equiaxed SiC microstructure [Lowden 2006; Gerczak et al. 2016]. In addition to the fact that AGR-1 fuel had smaller, 350-µm-diameter UCO kernels, notable differences in the TRISO particle properties included the pyrocarbon anisotropy, which was slightly higher in the particles coated in the engineering-scale coater, and the exposed kernel defect fraction, which was higher for AGR-2 fuel due to the detected presence of particles with impact damage introduced during TRISO particle handling [Hunn 2010].

Irradiation test compacts containing AGR-2 fuel particles were compacted at ORNL with the same resinated-graphite blend used to make AGR-1 compacts and a modified pressing process that utilized a die heated to 65°C and a new computer-controlled servo-press. Two compact lots were produced and qualified for the AGR-2 irradiation test: lot LEU09-OP2-Z contained the UCO TRISO particles [Hunn, Montgomery, and Pappano 2010a] and lot LEU11-OP2-Z contained the UO_2 fuel [Hunn, Montgomery, and Pappano 2010b]. Compared to the AGR-1 compacts, which were compacted at room temperature using a manual press, the modified AGR-2 compacting process produced compacts with reduced variability in length and higher matrix density (1.6–1.7 g/cc for AGR-2 versus 1.2–1.3 g/cc for AGR-1). Compilations of the properties data for the particles and compacts are available in pre-irradiation characterization summary reports for the AGR-1 [Hunn, Savage, and Silva 2012] and AGR-2 [Hunn, Savage, and Silva 2010] fuel composites.

The *AGR-2 Post-Irradiation Examination Plan* [Demkowicz 2013] includes safety testing of the irradiated compacts in the Oak Ridge National Laboratory (ORNL) Core Conduction Cooldown Test Facility (CCCTF) and the Idaho National Laboratory (INL) Fuel Accident Condition Simulator (FACS) to evaluate the effect of elevated temperature on fuel microstructure, individual particle coating failure, and overall fission product† retention. The safety tests typically involve heating compacts in flowing helium to maximum temperatures of 1600, 1700, or 1800°C and holding at these temperatures for

* The background text in this introduction section originally appeared in a previous AGR-2 PIE report [Hunn et al. 2016a].

† In this report, the term "fission product" is used in a general sense to refer to all the post-fission isotopes remaining at the end of the irradiation test. These include: isotopes directly generated by the fission process, isotopes generated by neutron capture, isotopes generated by radioactive decay, and residual uranium.

approximately 300 h. The standard test temperature of 1600°C is the expected maximum temperature during a high-temperature gas-cooled reactor (HTGR) depressurization conduction-cooldown event, while 1700°C and 1800°C tests explore the safety margin and provide additional data on mechanisms for particle coating failure, fission product diffusion, and other fission product interactions with the TRISO coatings.

The first two CCCTF AGR-2 safety tests were performed on AGR-2 UO_2 Compacts 3-3-2 and 3-4-2; both were heated to 1600°C in flowing helium for 300 h and results were summarized in a previous report [Hunn et al. 2015a]. These UO_2 compacts both exhibited SiC failure in multiple particles because of the CO generated from excess oxygen, which produced noticeable corrosion and fracture of the weakened SiC layer. This observed failure is in sharp contrast to the performance of the UCO compacts that have been safety tested thus far [Morris et al. 2016; Hunn et al. 2018], where CO production was mitigated by the oxygen gettering of the uranium carbide in the UCO kernels. Safety testing at 1600°C has been performed and previously reported on AGR-2 UCO Compacts 2-2-2, 2-3-1, 5-2-2, and 6-4-2 [Hunn et al. 2016a; Hunn et al. 2017], and there were no indications of cesium release related to SiC failure in these tests. Also previously reported were results from 1800°C safety testing on AGR-2 UCO Compact 5-4-1, where evidence pointed to the presence of one particle that released cesium because of localized palladium degradation of the SiC layer [Hunn et al. 2016a; Hunn et al. 2018].

In this report, results from 1800°C safety testing and post-safety-test PIE of AGR-2 UCO Compact 2-3-2 and 1700°C safety testing of AGR-2 UO_2 Compact 3-4-1 are discussed and compared to previously-reported results from 1800°C safety testing of AGR-2 UCO Compact 5-4-1 and 1600°C safety testing of compact "twins": AGR-2 UCO Compact 2-3-1 and AGR-2 UO_2 Compact 3-4-2. These compact pairs are called "twins" because their symmetric locations in the irradiation test train resulted in similar irradiation conditions. Table 1 shows the calculated burnup in percent fissions per initial metal atom (FIMA), the fast neutron fluence (neutron energies > 0.18 MeV), and the average compact temperatures during irradiation for these compacts. Capsule 2 Compacts 2-3-2 and 2-3-1 were intentionally irradiated at notably higher temperature than compacts in the other AGR-2 capsules or those previously studied in the AGR-1 irradiation test. The Capsule 2 compacts provide insight into the irradiation and post-irradiation safety test performance at higher temperatures than typical HTGR operating temperatures.

Table 1. Irradiation conditions for AGR-2 compacts discussed in this report

Compact ID [a]	Fabrication ID [b]	Fuel Type	Average Burnup [c] (%FIMA)	Fast Fluence [c] (n/m^2)	Temperature [d] (°C)
AGR-2 2-3-1	LEU09-OP2-Z125	UCO	12.63	3.42×10^{25}	1296
AGR-2 2-3-2	LEU09-OP2-Z066	UCO	12.68	3.46×10^{25}	1296
AGR-2 5-4-1	LEU09-OP2-Z028	UCO	12.05	3.12×10^{25}	1071
AGR-2 3-4-1	LEU11-OP2-Z188	UO_2	10.62	3.47×10^{25}	1013
AGR-2 3-4-2	LEU11-OP2-Z150	UO_2	10.69	3.50×10^{25}	1013

[a] The X-Y-Z compact identification (ID) convention denotes the location in the irradiation test train: Capsule-Level-Stack.
[b] Physical properties data for individual compacts are available and tabulated based on fabrication ID [Hunn, Montgomery, and Pappano 2010a, pages 60–69; Hunn, Montgomery, and Pappano 2010b, pages 73–84].
[c] Burnup [Sterbentz 2014, table 6] and fast fluence [Sterbentz 2014, table 12] are based on physics calculations.
[d] Time-averaged, volume-averaged (TAVA) irradiation temperature [Hawkes 2014, table 4] is based on thermal calculations.

2. RESULTS OF SAFETY TESTING AND POST-SAFETY-TEST PIE

Safety testing in the CCCTF furnace was accomplished with the same methods used for AGR-1 safety testing [Baldwin et al. 2012]. Compacts were placed in a graphite holder that positions the compact in the furnace and simulates the graphite that surrounds the compacts in a prismatic-block reactor. A water-cooled deposition cup located near the top of the tantalum-lined furnace chamber collected vaporized metallic elements that escaped from the compact and surrounding graphite holder. Deposition cups were periodically removed and replaced with a new cup using a maximum exchange interval of ~24 h and shorter exchange intervals for the first few cups removed after heating up to the test temperature. The cups were monitored with gamma spectrometry to track safety test progress, with particular emphasis on collected cesium inventory that would indicate SiC failure [Hunn et al. 2014a]. Gaseous fission products were collected from the helium sweep gas as it passed through a liquid-nitrogen-cooled trap that was monitored for ^{85}Kr because significant and rapid krypton release would indicate complete failure of a TRISO coating [Morris et al. 2014]. After completion of each safety test, additional analysis was performed to measure fission products on the deposition cups and other CCCTF furnace internals (graphite fuel holder, tantalum furnace liner, and tantalum gas inlet line). This allowed for the determination of the cumulative release from the compact of each detected fission product.

The cumulative deposition cup collection efficiency varied for different elements due to variability in the transport of the elements out of the graphite holder and onto the water-cooled cups. The cumulative release fraction of each fission product measured on the deposition cups at the end of the safety test is a measure of the average deposition cup collection efficiency. The deposition cup collection efficiency is expected to vary with time, but this time dependence cannot be determined by a single measurement at the end of the test. To estimate the time-dependent release of fission products from the compact, the collection efficiency was assumed to be constant. This is a fairly good estimate for some of the more volatile elements, such as cesium and silver, but is often inaccurate for other elements, such as europium and strontium. The slower transport of some elements to the deposition cups is often evident in the cumulative release fraction retained in the graphite holder or on the tantalum furnace internals as discussed in the following sections. Elements whose transport to the deposition cups is slow with respect to the deposition cup exchange interval will appear to have a greater time-dependent increase in the release rate, especially in the early stages of the safety test, due to the assumption of a constant cup collection efficiency.

Fission product measurements are reported as fractions of the total compact inventory using the standard AGR PIE approach described in [Hunn et al. 2013, page 6]. For this method, the total inventory of each isotope is estimated for each compact by physics calculations and tabulated for one day after the end of the irradiation, one year after the end of the irradiation, and two years after the end of the irradiation (AGR-2 calculated compact values come from [Sterbentz 2014]. Radioisotope quantities measured by gamma spectrometry (e.g., ^{85}Kr, ^{110m}Ag, ^{134}Cs, ^{137}Cs, ^{154}Eu, and ^{155}Eu) or chemical separation and beta spectrometry (e.g., ^{90}Sr) are decay-corrected to one day after the end of the irradiation and divided by the calculated total inventory at that time to determine the total-inventory fraction. For stable isotopes (e.g., ^{104}Pd) and actinides (e.g., ^{235}U, ^{236}U, ^{238}U, ^{239}Pu, and ^{240}Pu), the measured quantity is divided by the calculated total inventory at one year after the end of the irradiation. This is done because many stable isotope inventories increase significantly over the first year after removal from the reactor while further increase in the calculated inventories after one year is typically negligible and the mass spectrometry analysis is almost always performed after one year has passed because of the time required for the test train to cool down and be disassembled. Data is also sometimes reported in terms of the equivalent particle inventory or number of particle-equivalents. This is simply the total compact inventory fraction multiplied by the average number of particles per compact (3176 for AGR-2 UCO compacts and 1543 for AGR-2 UO_2 compacts [Hunn 2010]).

2.1 AGR-2 UCO COMPACT 2-3-2 COMPARED TO UCO COMPACTS 2-3-1 AND 5-4-1

Figure 1 shows the estimated time-dependent release of key isotopes from AGR-2 UCO Compact 2-3-2 during the 1800°C safety test and Table 2 shows the distribution of those fission products on the furnace internals at the end of the test. The cumulative fraction on the deposition cups at the end of the safety test (Table 2, Row 1) was used as an estimated collection efficiency for each individual cup to generate the time-dependent curves in Figure 1. The collection efficiency for silver and cesium was very high, and the amount of these isotopes measured on the graphite holder and tantalum parts after the test was probably dominated by contamination from the hot cell. The europium and strontium collection efficiencies were higher than usually observed in CCCTF tests. This was probably due to a combination of the high test temperature and the relatively high amount of these elements residing in the compact matrix and/or outer pyrolytic carbon (OPyC) in this Capsule 2 compact. The observation that the higher AGR-2 Capsule 2 temperatures, compared to other AGR-1 and AGR-2 capsules resulted in dramatically higher transport of europium and strontium through intact SiC during the irradiation test and that most of this was held up in the compacts' carbanaceous material outside of the SiC has been discussed in multiple papers and reports [e.g., Harp, Demkowicz, and Stempien 2016; Hunn et al. 2016b]; and this europium and strontium sequestered in the carbonaceous material is susceptible to release from the compact when compacts are heated to safety test temperatures [Hunn et al. 2016a, 2017, 2018; Morris et al. 2016].

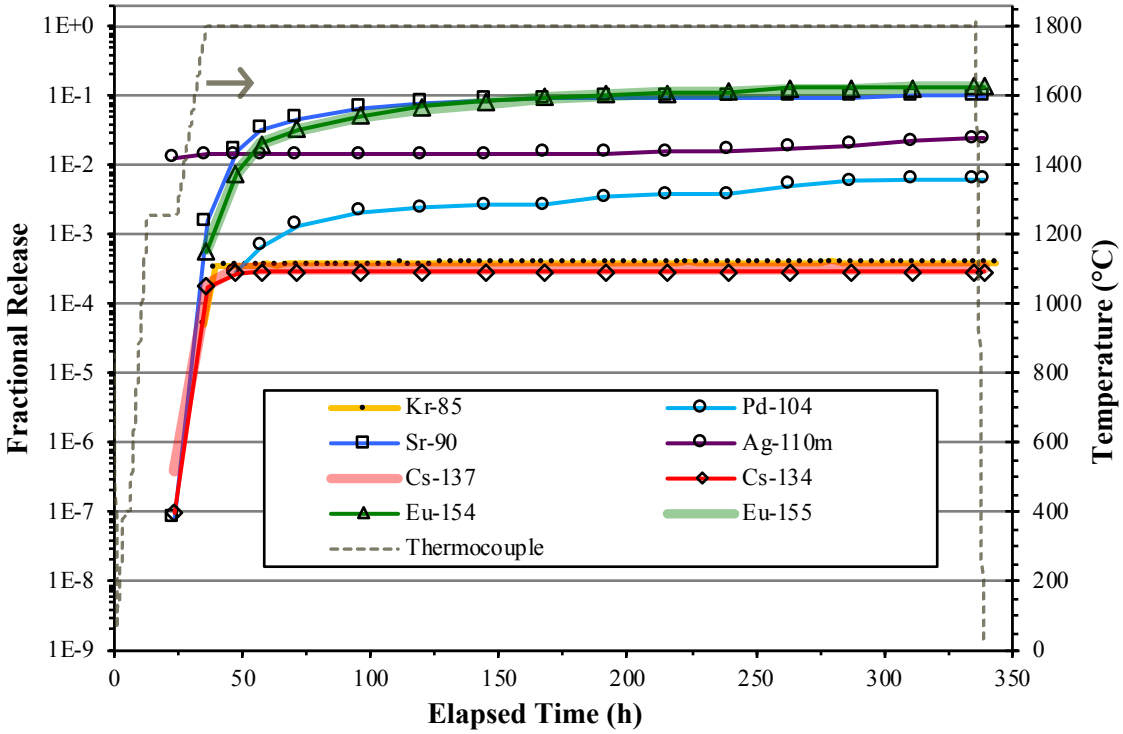

Figure 1. Release of fission products from Compact 2-3-2 during safety testing to 1800°C.

Table 2. Fission product distribution on furnace internal components after the Compact 2-3-2 safety test

Component	^{90}Sr	^{104}Pd	^{110m}Ag	^{134}Cs	^{137}Cs	^{154}Eu	^{155}Eu
Deposition cups	98.4%	82.8%	100%	98.9%	98.1%	87.8%	85.0%
Tantalum parts	1.4%	17.2%	~0%	1.1%	1.5%	8.7%	10.9%
Graphite holder	0.27%	~0%	~0%	~0%	0.33%	3.5%	4.1%

2.1.1 Silver Release

For comparison to the 1800°C safety test results for Compact 2-3-2, Figure 2 shows the previously reported results for Compact 2-3-1, which was safety tested at 1600°C [Hunn et al. 2017]. These compact twins showed similar levels of silver release early in the test, presumably because of their being similar inventories of silver sequestered in the compact matrix and OPyC at the end of the irradiation. Gamma measurements of the whole compacts showed 6.8% (-0.8%, +4.0%) of the calculated total ^{110m}Ag inventory was retained in Compact 2-3-2 and 16.0% (-1.1%, +1.7%) was retained in Compact 2-3-1 [Harp, Demkowicz, and Stempien 2016], but this whole-compact gamma scan data does not differentiate between ^{110m}Ag inside or outside of the SiC. For both compacts, the early time-dependent release behavior was the typically-observed rapid release of silver from the compact matrix and/or OPyC as compacts were brought to the safety test temperature followed by relatively-negligible additional release as the safety test progressed. However, Compact 2-3-2 showed additional ^{110m}Ag release during the latter portion of the test that indicates silver release through intact SiC was occurring at 1800°C. This 1800°C safety test release of ^{110m}Ag through intact SiC is common to AGR test fuel with fine-grain SiC deposited with an argon-diluent [Demkowicz et al. 2015, page 66], which was the deposition method for all AGR-2 TRISO particles [Phillips, Barnes, and Hunn 2010]. Silver release at 1800°C has been verified by 600-h heating tests of individual particles, where particles were observed to release almost all their silver inventory by the end of the test [Hunn et al. 2016c].

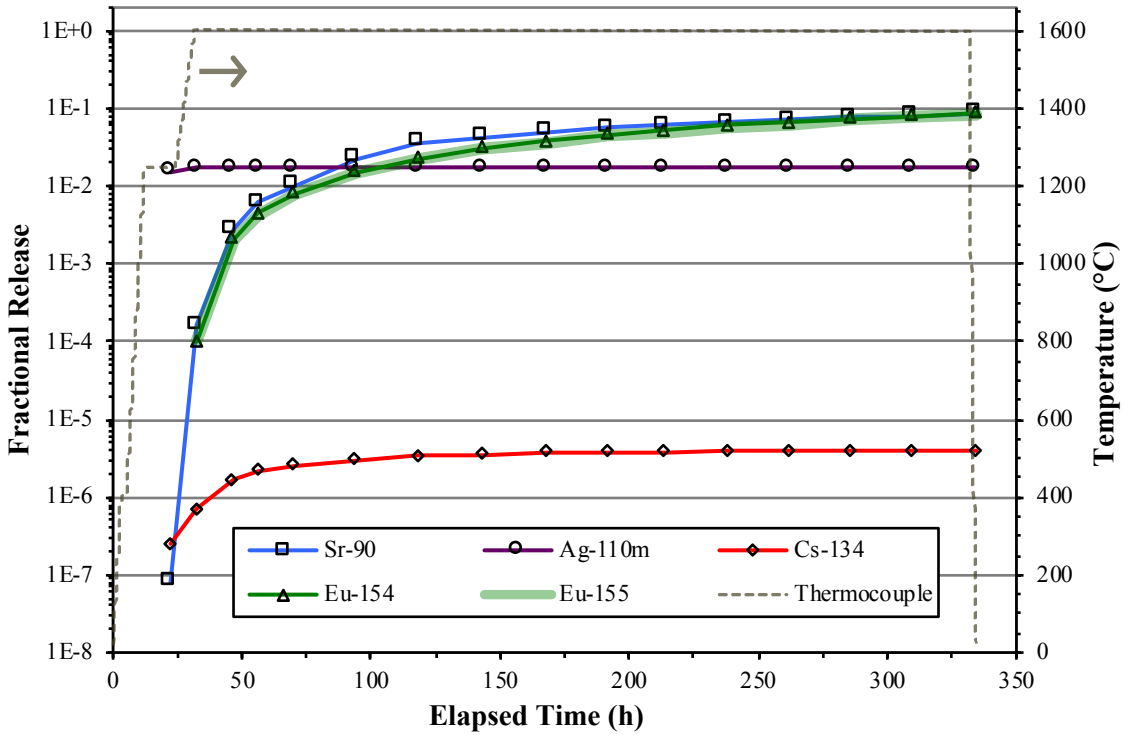

Figure 2. Release of fission products from Compact 2-3-1 during safety testing to 1600°C [Hunn et al. 2017].

The ^{110m}Ag release observed in the latter portion of the Compact 2-3-2 test was not as significant as what was observed in the 1800°C safety test of AGR-2 UCO Compact 5-4-1 (Figure 3) because Compact 2-3-2 had a much lower inventory of ^{110m}Ag in the particles at the start of the test. Figure 4 and Figure 5 show the ORNL Irradiated Microsphere Gamma Analyzer (IMGA) measurements of ^{110m}Ag in particles deconsolidated from these two compacts after the safety tests. Data is plotted as the measured versus calculated (M/C) ratio defined by the inset equation and processed as described in [Hunn et al. 2013]. All

but four of the analyzed Compact 2-3-2 particles had ^{110m}Ag inventories below the ^{110m}Ag M/C quantification limit of 14–22%, while most Compact 5-4-1 particles had significant ^{110m}Ag inventory remaining. The Compact 2-3-1 ^{110m}Ag distribution measured with IMGA was similar to Compact 2-3-2 (Figure 6) but a larger fraction of low-silver particles could be measured because the earlier analysis of the Compact 2-3-1 particles provided a lower detection limit.

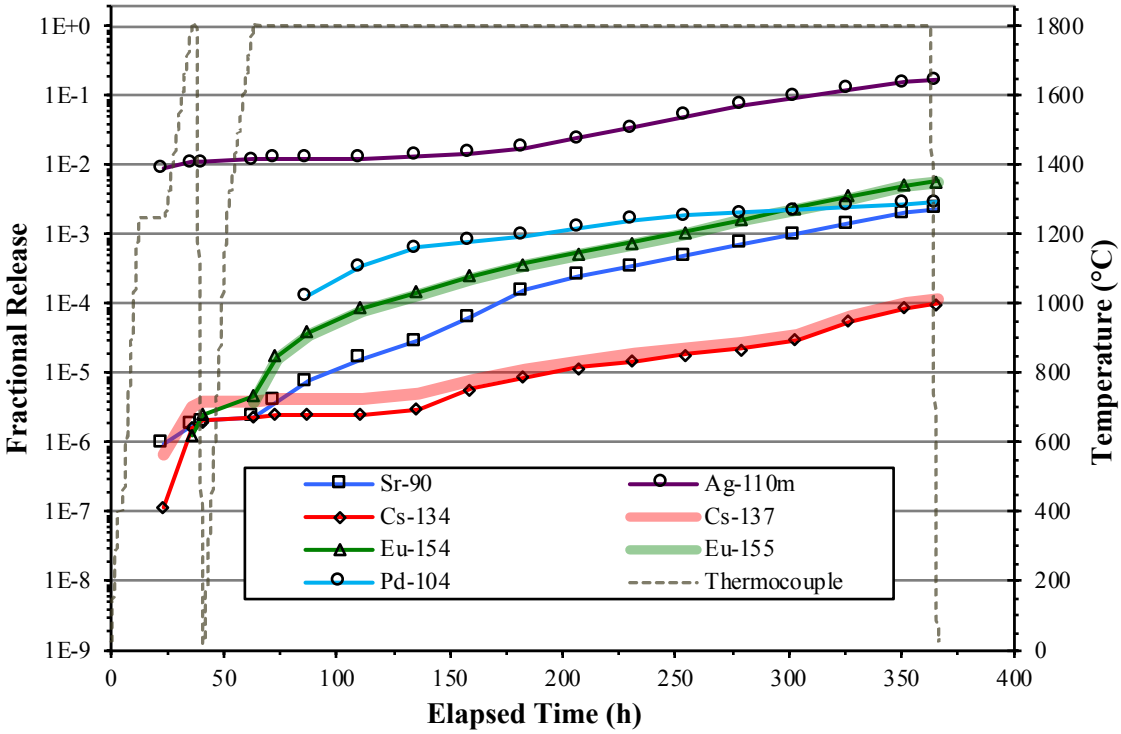

Figure 3. Release of fission products from Compact 5-4-1 during safety testing to 1800°C [Hunn et al. 2016a].

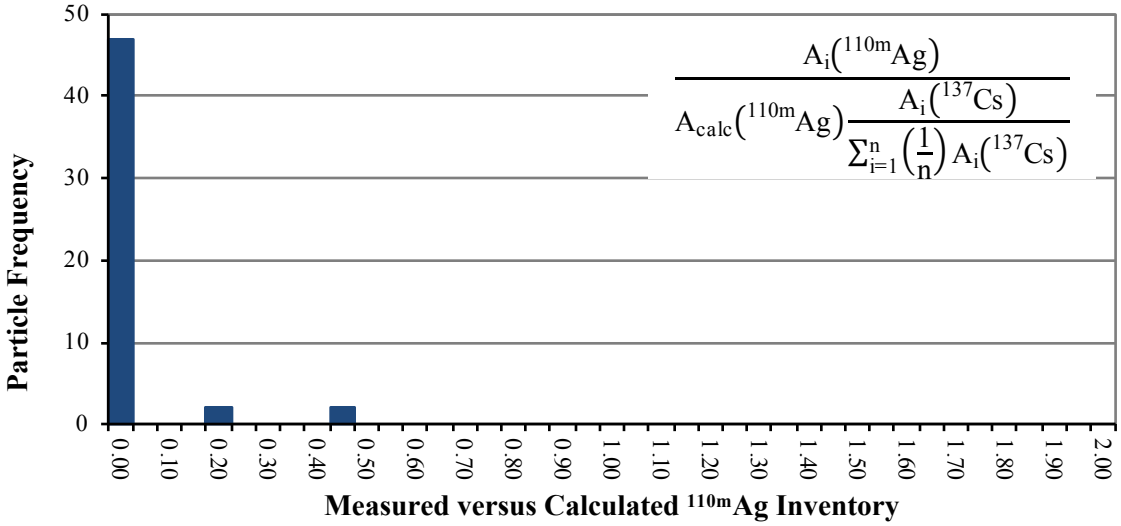

Figure 4. Ratio of ^{110m}Ag retained in 51 randomly-selected Compact 2-3-2 particles after safety testing to 1800°C versus the calculated inventory, adjusted for variation in fissionable material and burnup with the measured ^{137}Cs activity (particles plotted as "zero" were below a detection limit of ^{110m}Ag M/C < 14–22%).

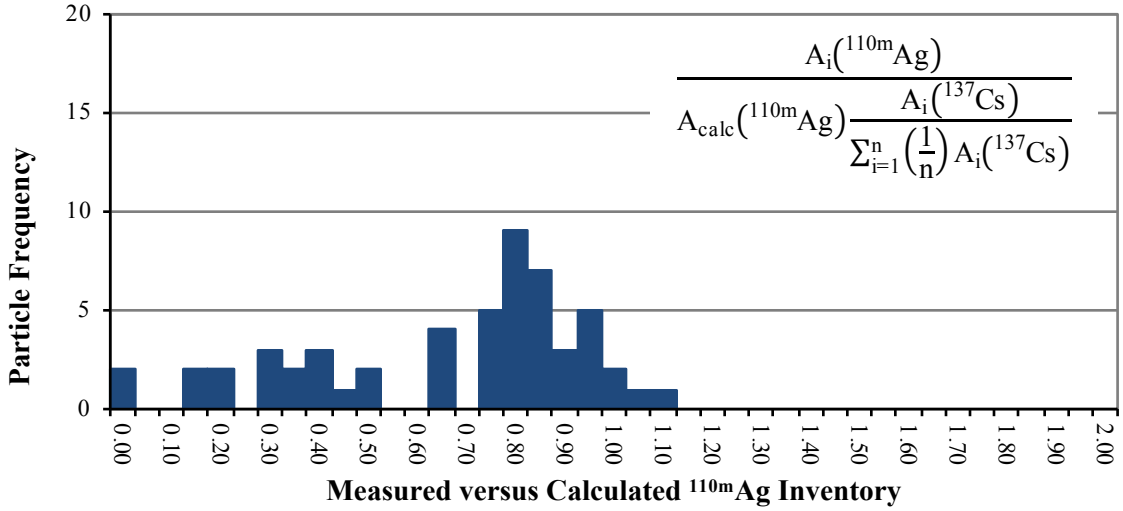

Figure 5. Ratio of ^{110m}Ag retained in 54 randomly-selected Compact 5-4-1 particles after safety testing to 1800°C versus the calculated inventory, adjusted for variation in fissionable material and burnup with the measured ^{137}Cs activity (particles plotted as "zero" were below the detection limit of ^{110m}Ag M/C < 12–13%.

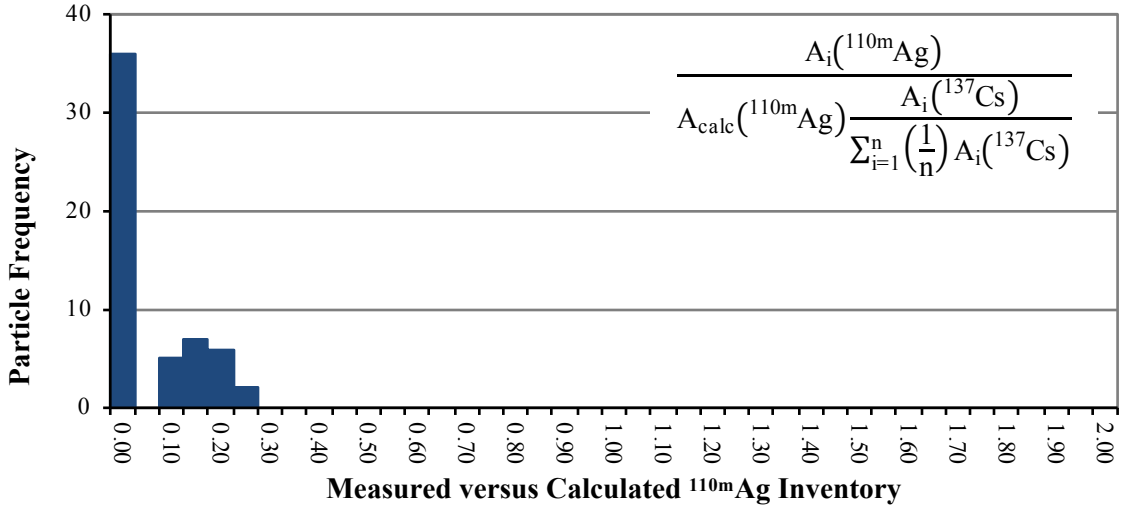

Figure 6. Ratio of ^{110m}Ag retained in 56 randomly-selected Compact 2-3-1 particles after safety testing to 1600°C versus the calculated inventory, adjusted for variation in fissionable material and burnup with the measured ^{137}Cs activity (particles plotted as "zero" were below the detection limit of ^{110m}Ag M/C ≲ 9–13%.

2.1.2 Cesium and Krypton Release and Observed Particle Failure

Figure 2 shows that very little ^{134}Cs was detected on the deposition cups from the 1600°C safety test of Compact 2-3-1. This may have been from very small amounts of ^{134}Cs in the compact matrix and/or OPyC or may be from hot cell contamination that can be picked up on the compact surface, graphite holder, or deposition cups when they are handled in the hot cell. In contrast, Figure 1 shows that there was a significant cesium release from Compact 2-3-2 as it was heated to 1800°C, reaching a level close to the compact inventory fraction in an average particle (one particle-equivalent equals 3.15E-4). A similar amount of ^{85}Kr was released concurrently. The cumulative ^{85}Kr activity in the sweep gas trap reached about 1.1 particle-equivalents of ^{85}Kr within the first four hours at 1800°C, at which time the release rate slowed by about two orders of magnitude. This combination of cesium and krypton release suggests the presence of a particle with failed TRISO.

After safety testing, Compact 2-3-2 was subjected to deconsolidation and leach-burn-leach analysis (DLBL) using the process described in [Hunn et al. 2013] with one modification. After deconsolidation, the two pre-burn leaches in the Soxhlet extractor were skipped to try to minimize particle damage prior to the hot acid digestion and sieving steps used to clean remaining matrix off of the TRISO particles and separate the particles from the matrix debris for IMGA survey. This was done because of previous observation of particle coating failure during the Soxhlet extractions. However, the deconsolidation and digestion process can also result in broken coatings as a result of matrix removal and handling of particles that have apparently been weakened by the irradiation and/or safety testing. The post-burn matrix leach results in Table 3 indicate that post-safety test coating damaged occurred and kernels were exposed during the deconsolidation and digestion of Compact 2-3-2 that were most likely not exposed during the safety test. While some cerium, uranium, and plutonium can be expected to migrate through intact SiC during irradiation and safety testing (especially for Capsule 2 compacts), cesium is well-retained when SiC remains intact. When DLBL was performed on as-irradiated Compact 2-2-1, which had irradiation conditions similar to Compact 2-3-2 and no particles with failed layers, there were moderate particle-equivalents of exposed ^{144}Ce (1.4), ^{238}U (0.69), and ^{239}Pu (1.1) in the leach solutions, but very little ^{134}Cs (0.013 particle-equivalents) [Hunn et al. 2018]. Table 3 shows that there were around 3 particle-equivalents of ^{134}Cs and ^{137}Cs detected in the post-burn matrix leachate from Compact 2-3-2, which suggests layers were fractured and kernels exposed during the deconsolidation and digestion process.

Table 3. Exposed particle-equivalents of various isotopes detected by DLBL

LBL Step	Post-burn matrix leach after digestion and sieving [a]	Post-burn particle leach 1	Post-burn particle leach 2
^{90}Sr	4.67	0.49	0.009
^{106}Ru	1.38	0.17	0.007
^{110m}Ag	<4.3	<1.7	<0.32
^{125}Sb	3.30	0.86	0.058
^{134}Cs	2.99	0.22	0.012
^{137}Cs	3.27	0.29	0.018
^{144}Ce	9.81	1.69	0.066
^{154}Eu	6.11	1.48	0.049
^{155}Eu	5.89	1.72	0.051
^{235}U	7.26	0.35	0.009
^{236}U	6.90	0.31	0.006
^{238}U	6.77	0.30	0.012
^{239}Pu	9.21	1.94	0.073
^{240}Pu	11.5	3.21	0.12

[a] Only one post-burn matrix leachate was analyzed due to second post-burn matrix leach vessel breaking when dropped. Because the Soxhlet extractions were skipped, the post-burn matrix leachate includes isotopes that would normally be detected separately in the pre-burn leaches.

An IMGA survey of particles from Compact 2-3-2 found one particle (Particle 232-SP01) with only 2% of the cesium inventory in an average particle. The amount of cesium released from this particle could account for the amount of cesium released during the safety test. Six-hour gamma counting showed that Particle 232-SP01 also had low inventories of ^{125}Sb (17%) and ^{154}Eu (6%) but high inventories of ^{106}Ru (113%) and ^{144}Ce (64%), relative to an average particle. X-ray tomography of this particle showed OPyC and SiC degradation that looked like it started from outside the particle. Figure 7 shows the region where the SiC and OPyC layers were clearly compromised. Some degradation features were also visible in the inner pyrolytic carbon (IPyC) layer adjacent to the degraded SiC, but the x-ray tomography could not clearly resolve obvious through-layer fracture of the IPyC, only degradation similar to the OPyC.

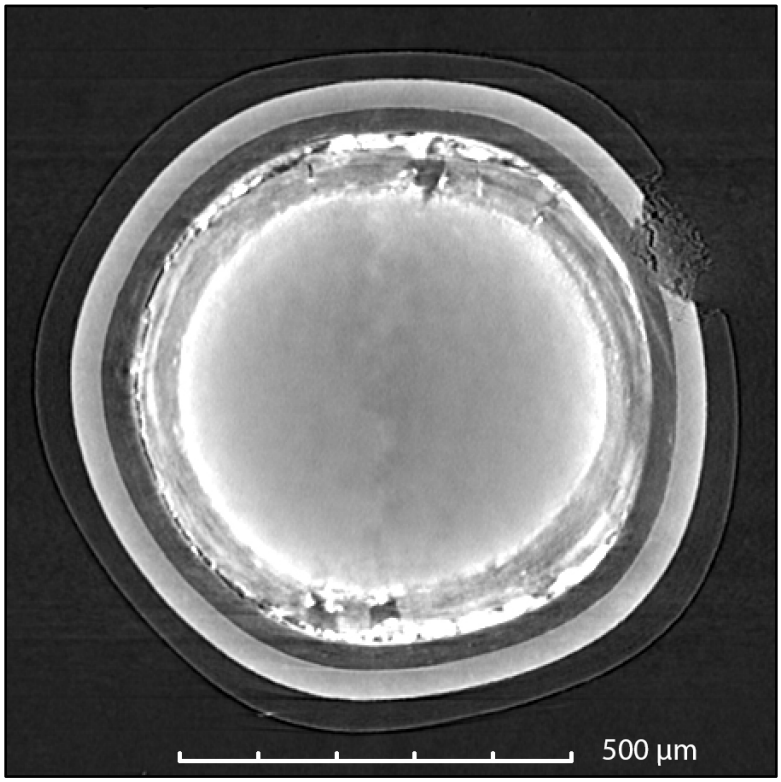

Figure 7. X-ray tomogram of Particle 232-SP01 from 1800°C safety-tested Compact 2-3-2.

In Figure 7, the relatively-high brightness in the buffer region and at the buffer/IPyC interface indicates the presence of material with high atomic number (Z). Analysis by scanning electron microscopy (SEM) with energy-dispersive x-ray spectroscopy (EDS) identified this to be predominantly uranium. Similar uranium dispersion was observed in five particles whose TRISO layers failed to retain cesium and krypton during a 650-h test at 1800°C of particles deconsolidated from AGR-1 UCO Compact 4-4-2 [Hunn et al. 2015b]. Like Particle 232-SP01, the five failed-TRISO particles from Compact 4-4-2 released all but 1% of their Cs and most of their ^{125}Sb and ^{154}Eu but retained all their ^{106}Ru. Retention of ^{144}Ce in the Compact 4-4-2 failed-TRISO particles varied, possibly because of the different amount of time each particle was at temperature after TRISO failure occurred. Particle 442-A009 retained 61% of its ^{144}Ce, similar to Particle 232-SP01. As discussed in the Compact 4-4-2 loose-particle test report [Hunn et al. 2015b, page 20], uranium dispersion into the buffer at 1800°C has been observed before and can be related to the loss of a particle's ability to retain carbon monoxide. Studies have shown that carbon reduction of uranium oxide can proceed at 1800°C if a sufficient partial pressure of carbon monoxide is not present [Wilhelm 1964]. This instability of the buffer/kernel system in particles with failed TRISO is a probable explanation for the observed uranium dispersion in these failed-TRISO particles.

Further analysis by grinding and polishing Particle 232-SP01 to reveal a section through the localized degraded region was performed. Figure 8 shows optical micrographs of several planar sections that were acquired as the central region of the degradation was approached. It is evident that a reaction occurred at this site that thoroughly destroyed the SiC. There is also evidence that reactions occurred that degraded the pyrocarbon in this region. Some areas of the OPyC were missing, perhaps having crumbled away during the deconsolidation and acid digestion process. For the polish plane shown in Figure 8d, some of the material filling the degraded region was wiped away by the cleaning process prior to final imaging of the polished surface (it was originally flush with the surface of the mount).

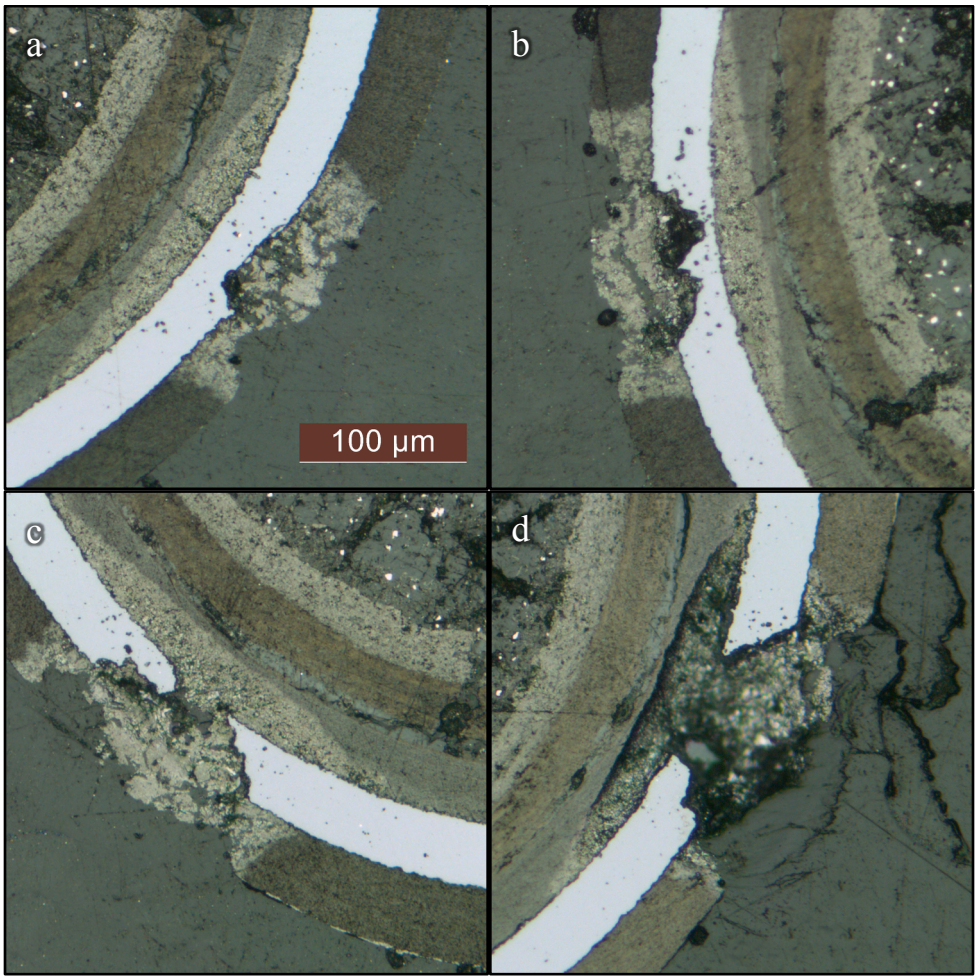

Figure 8. Optical micrographs of degraded SiC region in Particle 232-SP01 from 1800°C safety-tested Compact 2-3-2 viewed in several planes as material was removed (progressing in time from a to d).

Figure 8 and Figure 9 show several fractures in the buffer and detachment of the buffer from the IPyC, except for a section immediately adjacent to the degraded region. This may be significant in that IPyC fracture often occurs at the boundary between detached and attached buffer. In Figure 8 and Figure 9, the different appearing material in and around the degradation site indicates the presence of a reaction byproduct. The material in the inner half of the buffer also appears discolored, and the kernel material appears granular with some kernel material missing (Figure 9). The discolored band around the inner half of the buffer is apparently from dispersion of uranium reacting with the buffer and uranium-rich material filling the buffer porosity in that band. Figure 10 is a scanning electron image (SEI) of one section of the buffer that shows dense, uranium-rich features in the buffer pores, while the outer half of the buffer still shows open porosity.

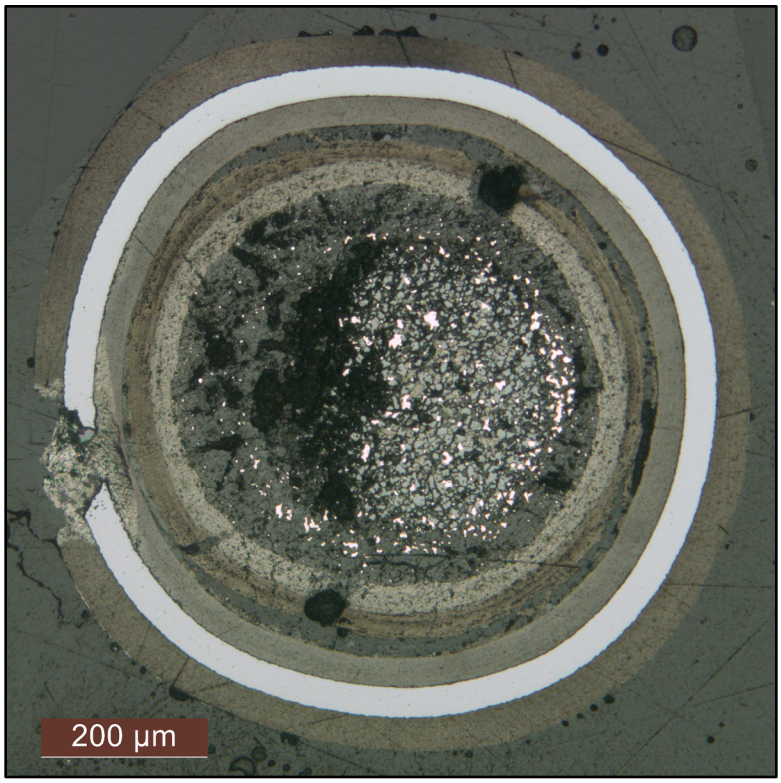

Figure 9. Optical micrograph of Particle 232-SP01 planar section prior to final polish.

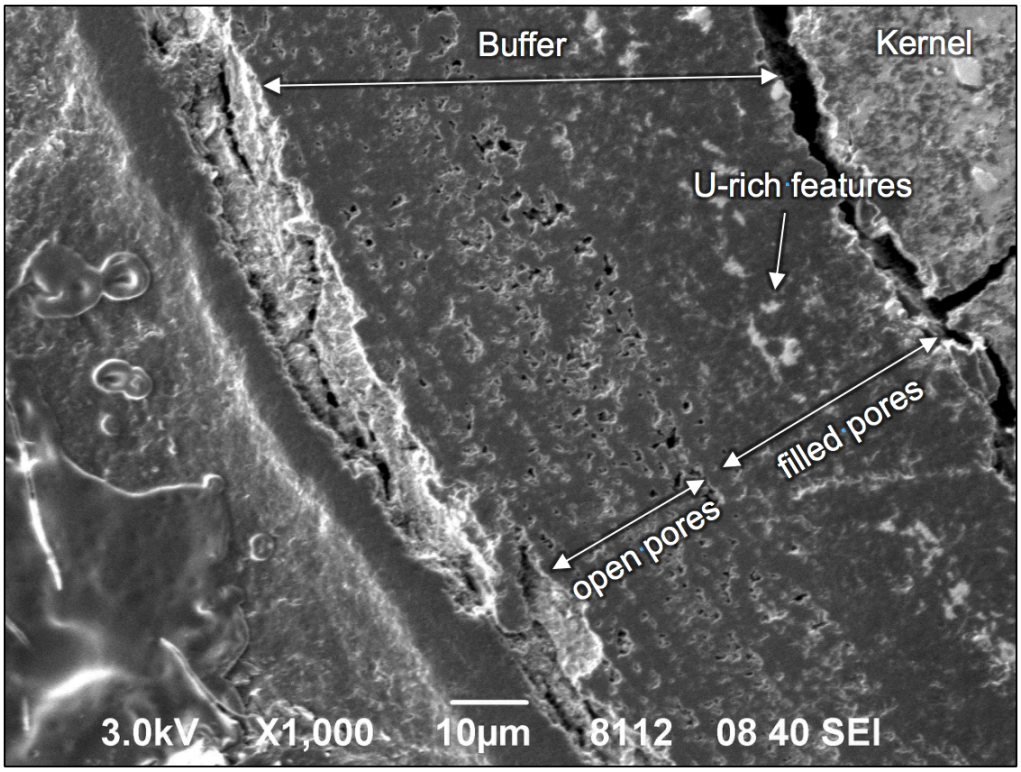

Figure 10. Electron micrograph of Particle 232-SP01 planar section showing demarcation between an inner region with pores filled with U-rich material and an outer region without.

Figure 11 is a backscattered electron/scanning electron composite (BEC) image that highlights the high-Z material surrounding the degraded region. Various features are labeled in the figure, but the key feature is the predominance of molybdenum observed around the degraded region. Molybdenum is a likely candidate for reaction with both carbon and SiC at 1800°C. Molybdenum is also a possible foreign contaminant in the fuel. The hot-sampling cup in the 150-mm coater used to deposit the AGR-2 TRISO coating was made of molybdenum. During SiC soot inclusion analysis of 3510 particles from the BWXT AGR-2 UO2 irradiation test fuel TRISO composite G73H-10-93085B used to make the AGR-2 UO_2 compacts, one particle was identified with a molybdenum inclusion in the SiC [Hunn 2009]. Figure 12 and Figure 13 are images from the inspection report. A bulge in the SiC layer is evident indicating the molybdenum inclusion had sufficient bulk to impact the layer thickness in that region.

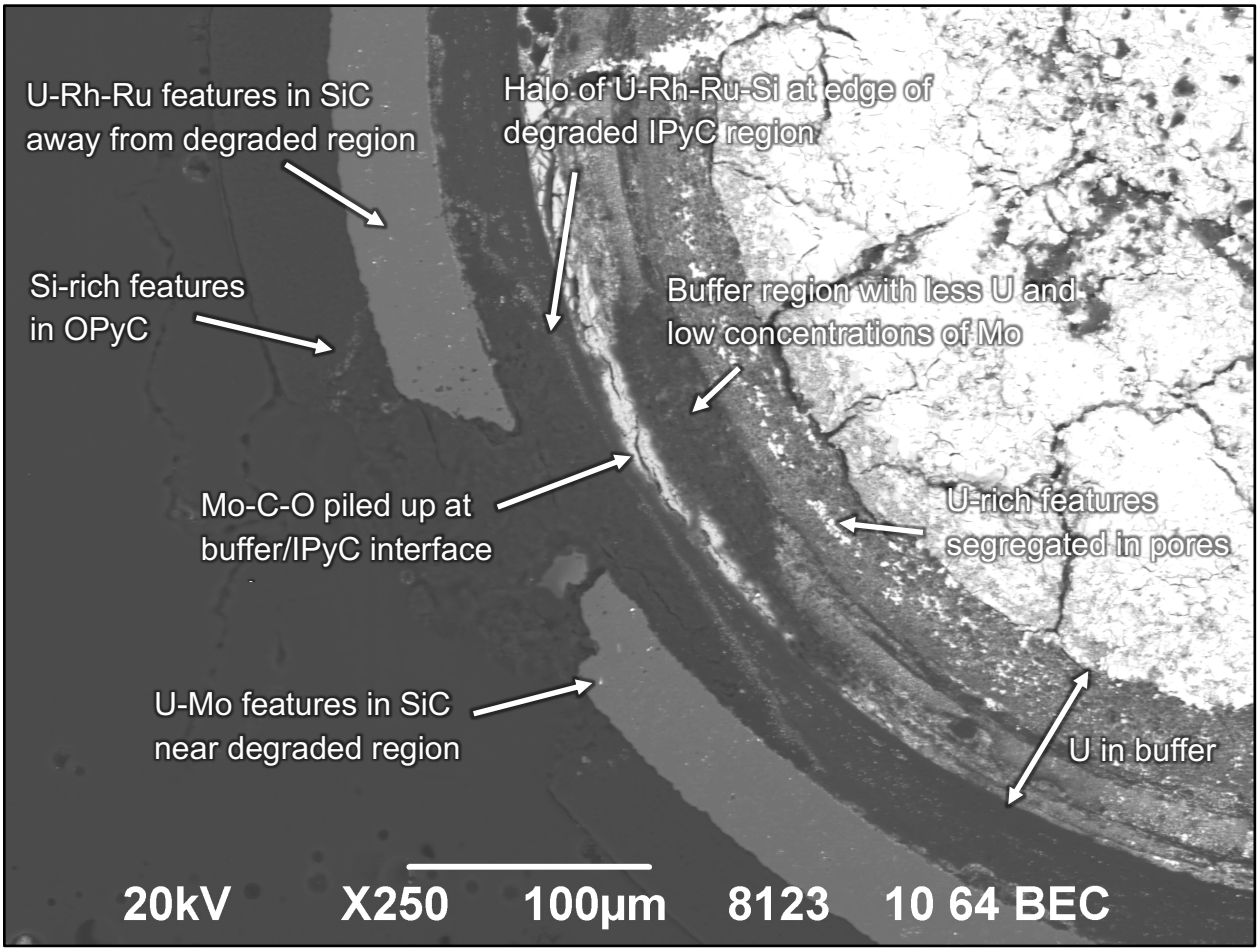

Figure 11. Electron micrograph of Particle 232-SP01 planar section showing area around degraded region.

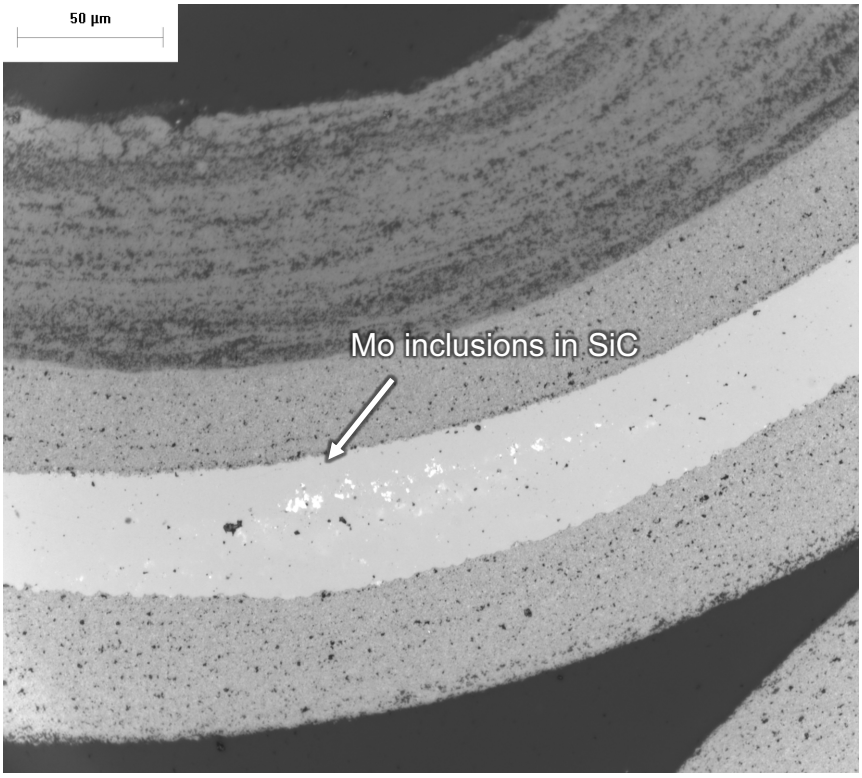

Figure 12. Optical micrograph of AGR-2 UO_2 TRISO showing molybdenum inclusion in SiC [Hunn 2009].

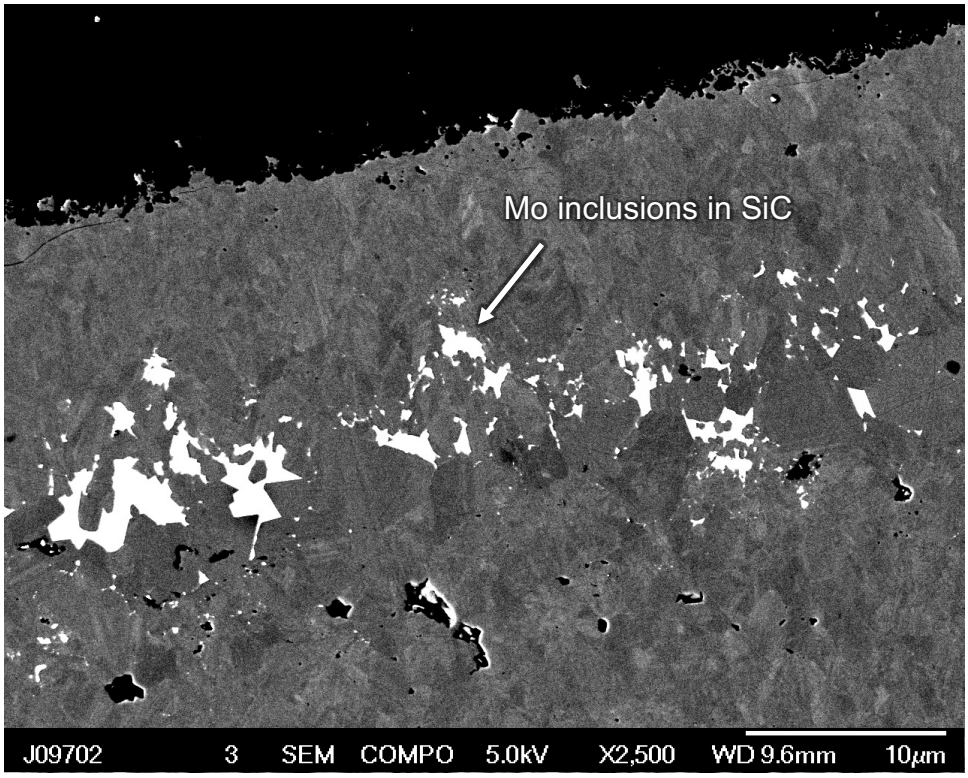

Figure 13 Electron micrograph of AGR-2 UO_2 TRISO showing molybdenum inclusion in SiC [Hunn 2009].

The observed microstructure of failed Particle 232-SP01 was clearly different from that of failed Particle 541-SP02 shown in Figure 14. Particle 541-SP02 SiC failure was caused by the same type of fission product degradation observed multiple times in AGR-1 test fuel. Figure 14 shows numerous bright spots in the SiC surrounding the degredation site that were determined to be predominantly uranium (presumably palladium was present at some point but had diffused away at 1800°C). The darker spots in the SiC are carbon-rich areas left behind by the conversion of the SiC to silicide that subsequently diffused away. The tapered shape of the degradaded region in Particle 541-SP02 indicates a progression of the degradation from the IPyC/SiC interface to the outer boundary of the SiC. In contrast, the shape of the degradaded region in Particle 232-SP01 was tapered in the other direction.

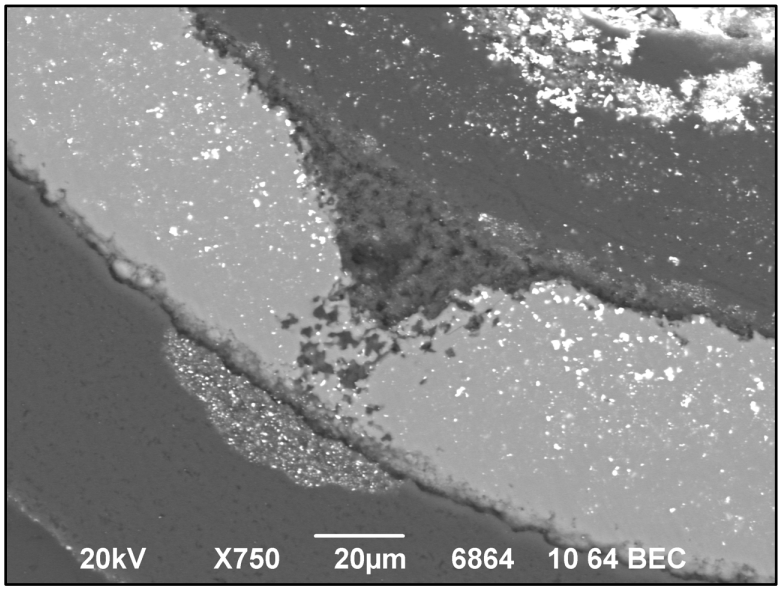

Figure 14. Electron micrograph of failed-SiC particle from 1800°C safety-tested Compact 5-4-1 showing region of degraded SiC with bright spots indicating clusters of higher-Z elements.

Figure 15 and Figure 16 are derived from the same data from the Compact 2-3-2 and Compact 2-3-1 safety test used to generate Figure 1 and Figure 2, respectively, with the data in Figure 15 and Figure 16 plotted as the estimated average release rate during each deposition cup residence period instead of the cumulative release. Breaks in the plotted values are where the cup activities for a given fission product were too low to measure. Compact 2-3-1 showed a small spike in the ^{134}Cs release rate that peaked near 1E-7. As already mentioned, this may be from very small amounts of ^{134}Cs in the compact matrix and/or OPyC or may be from hot cell contamination that can be picked up on the compact surface, graphite holder, or deposition cups when they are handled in the hot cell. Compact 2-3-2 showed a larger spike in the ^{134}Cs release rate that peaked near 1E-5 and then returned to a background level of 1E-8, similar to the background level observed for Compact 2-3-1. This indicates that the particle failure that caused the observed cesium release during the Compact 2-3-2 safety test was either already present at the start of the test, occurred during heating to 1800°C, or happened within the first hour at 1800°C (when the second deposition cup was removed). It is significant that the cesium release from Compact 2-3-2, after the initial release, remained low throughout the remainder of the test because previous AGR-1 safety tests at 1800°C, where palladium degradation was observed to cause SiC failure, typically showed cesium release from this failure mechanism later in the test [Demkowicz et al. 2015, Figure 46]. The cesium release from the AGR-2 Compact 5-4-1 1800°C safety test (Figure 3) was consistent with the timing of particle failure observed in AGR-1 safety testing.

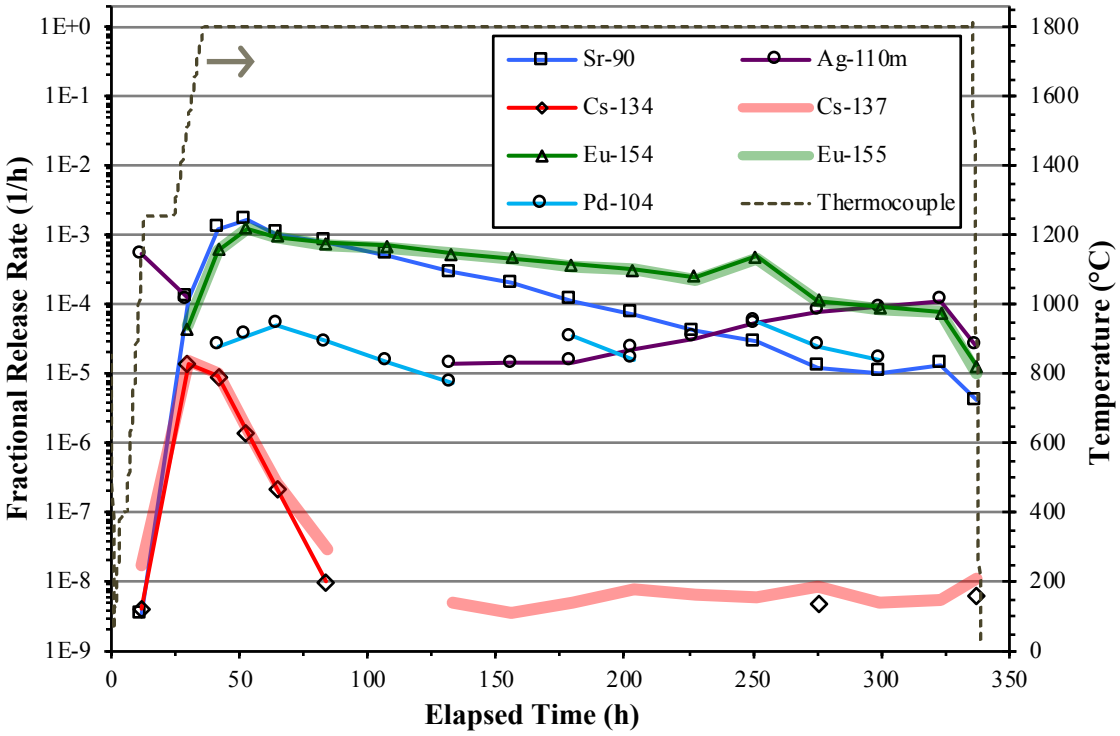

Figure 15. Rate of fission product release from Compact 2-3-2 during safety testing to 1800°C (data points with no measurable release rate are not plotted).

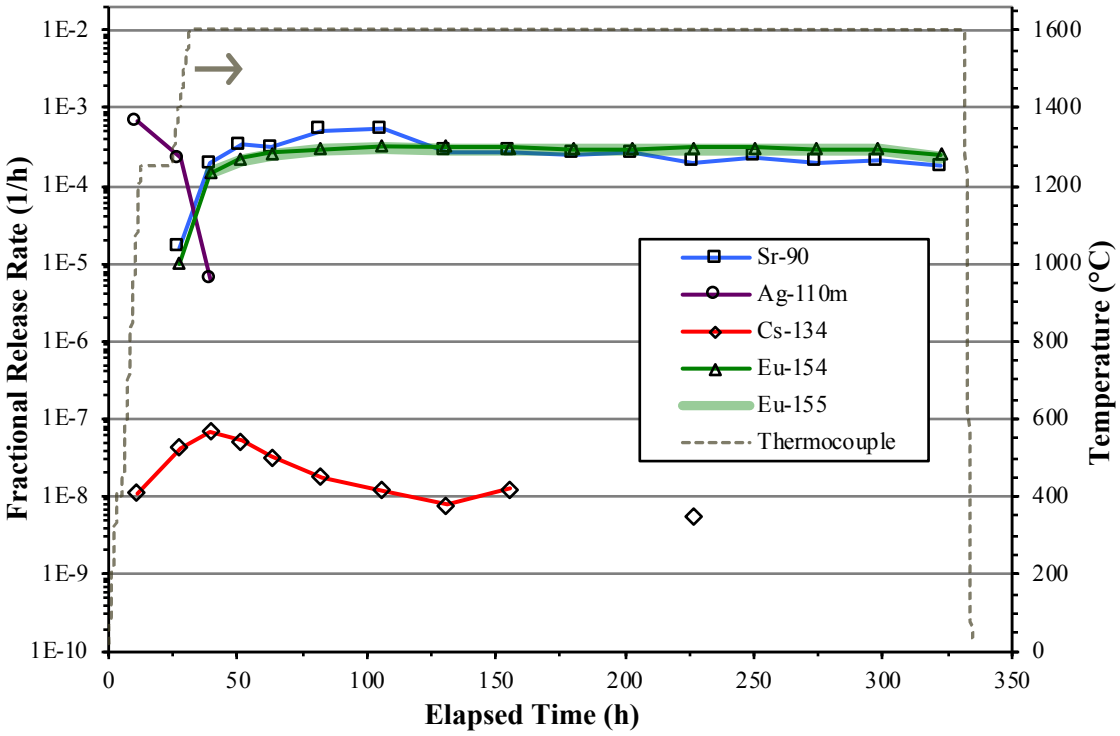

Figure 16. Rate of fission product release from Compact 2-3-1 during safety testing to 1600°C [Hunn et al. 2017] (data points with no measurable release rate are not plotted).

2.1.3 Strontium, Europium, and Palladium Release

Strontium and europium release during the 1800°C safety test of Compact 2-3-2 reached cumulative compact inventory fractions around 10% (Figure 1). Strontium and europium release during the 1600°C safety test of Compact 2-3-1 also reached cumulative compact inventory fractions around 10%, but it took longer for it to get to the cups (Figure 2). As discussed at the beginning of Section 2.1, this high fractional release during safety testing is mostly the result of high fractional release through intact SiC during irradiation, because most of the europium and strontium released through intact SiC during irradiation is sequestered in the matrix and/or OPyC until the elevated safety test temperatures cause it to be move out of the compact. Figure 15 shows that, during the Compact 2-3-2 safety test, the deposition cup collection rate for strontium and europium continuously decreased after the fourth cup was removed (~22 h after reaching 1800°C), while the rates during the Compact 2-3-1 safety test were lower but more constant (Figure 16). This is related to the rate that these elements were migrating to the cups and the fact that the strontium and europium were being depleted from the matrix and OPyC of Compact 2-3-2 as a result of the higher transport rate at 1800°C. By the end of the 1800°C safety test of Compact 2-3-2, there was only 5.2 particle-equivalents of ^{90}Sr and 7.6 particle-equivalents of ^{154}Eu remaining in the matrix and OPyC (Table 3), which was <2% of the total amount detected outside of intact SiC. At the end of the 1600°C safety test of Compact 2-3-1, there was still 30% of the exposed ^{90}Sr and 47% of the exposed ^{154}Eu remaining in the compact matrix and OPyC.

Figure 1 and Figure 3 show significant palladium release during the 1800°C safety tests of Compact 2-3-2 and Compact 5-4-1. Palladium release from a compact during 1600°C safety testing is typically too low to measure reliably, as was the case for Compact 2-3-1. However, at 1800°C, palladium sequestered in the compact matrix and OPyC at the end of the irradiation can more readily exit the compact, similar to strontium and europium. It has also been observed with SEM and EDS that palladium trapped in the SiC at the end of the irradiation is apparently released during 1800°C safety testing [Hunn et al. 2014b, pages 23–24]. Figure 1 and Figure 3 both show increases in the latter part of the test that suggest an initial release from the matrix and OPyC followed by additional release from, and possibly through, the SiC. Electron microscopy and elemental analysis of a few of the randomly-selected (RS) particles subjected to six-hour gamma scanning with IMGA (Figure 4) provides further evidence that transport of various species was occurring in the SiC at 1800°C

The SEM/EDS analysis of average particles from Compact 2-3-2 showed features with high Z (uranium, palladium, and other fission products) across the entire SiC layer and pileup of these features at the boundary between the IPyC and the SiC and in the interface region surrounding the IPyC/SiC boundary (where SiC tendrils extend into the IPyC). These features appear as bright spots in Figure 17, which shows a typical area of the polished section through Particle 232-RS16. Three features classes were observed in the SiC layer of the Compact 2-3-2 particles taken from the random IMGA sample: uranium-only features, uranium-with-trace-palladium features, and palladium-uranium features (with similar palladium and uranium intensities). The predominant features in the SiC layer were the uranium-rich feature classes of uranium-only and uranium-with-trace-palladium. The palladium-uranium features that were observed were more prevalent closer to the SiC/OPyC interface. The analyzed features at the IPyC/SiC boundary were palladium-uranium features and uranium-rich features (uranium-only and uranium-with-trace-palladium). Some uranium-rich features at the IPyC/SiC boundary also contained zirconium. The features in the IPyC/SiC interface region were primarily palladium-uranium. The palladium-uranium features near the IPyC/SiC interface, including those present in the SiC layer, often contained measurable rhodium concentrations.

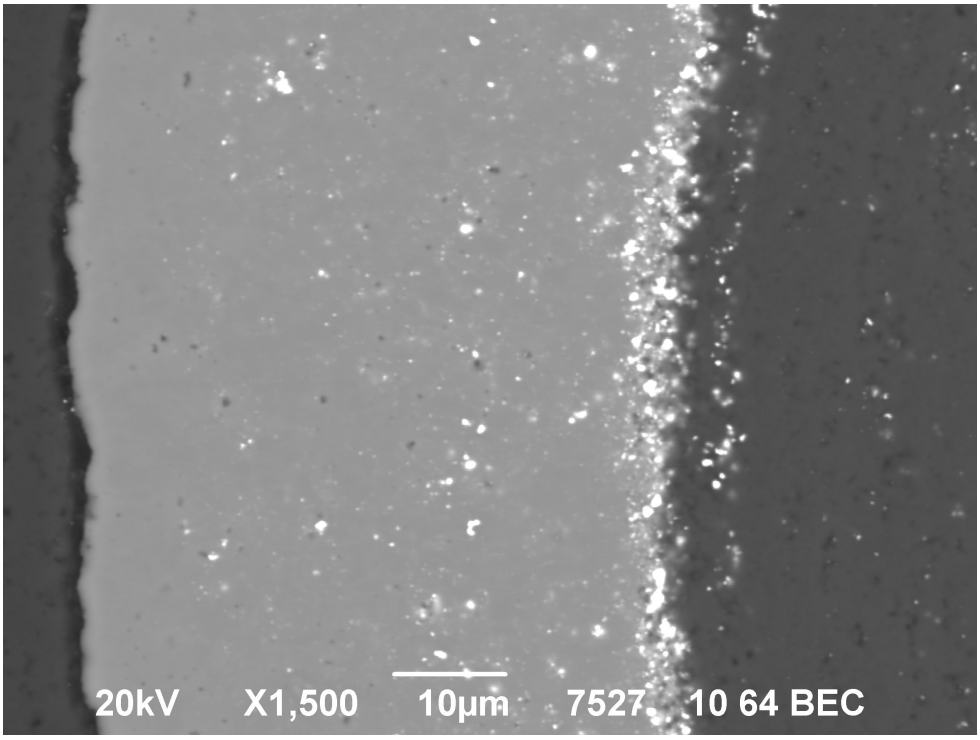

Figure 17. Electron micrograph of Particle 232-RS16 polished section showing (from left to right) OPyC, SiC with isolated high-Z features, IPyC/SiC interface region with pileup of high-Z features, and IPyC with isolated high-Z features.

Comparison of average Compact 2-3-2 particles with Compact 2-3-1 particles provides insight on the impact of safety test temperature on fission product transport in TRISO particles. Similar to what was observed in the Compact 2-3-2 particles, the SEM analysis of average particles from 1600°C safety-tested Compact 2-3-1 showed high-Z features across the SiC layer and piled up at the IPyC/SiC boundary and interface (Figure 18), but their composition and concentration differed significantly. The features piled up at or near the IPyC/SiC boundary in Compact 2-3-1 particles were predominantly palladium-uranium features, as observed in Compact 2-3-2 particles, but the presence of uranium at the interface was greater for particles in Compact 2-3-2. The features observed in the SiC layer of Compact 2-3-1 particles were primarily palladium-rich with trace or relatively-low concentrations of uranium. This was in contrast to the predominance of uranium-rich features observed in the SiC of the Compact 2-3-2 particles. A higher concentration of uranium at the IPyC/SiC interface and throughout the SiC in the 1800°C safety-tested particles, compared to the particles from the twin compact tested at 1600°C, indicates that uranium was migrating to and through the SiC at a measurably higher rate at 1800°C. This observation is consistent with the conclusion that the greater amount of uranium measured in DLBL of Compact 2-3-2 (Table 3) was at least partly due to greater diffusive release through intact particles at the higher safety test temperature.

The observation of a lower palladium intensity in the high-Z features in the SiC layer of Compact 2-3-2 particles compared to Compact 2-3-1 implies that palladium was also diffusing through the SiC much more readily at 1800°C. The fact that features in the SiC of Compact 2-3-2 particles that still had measurable palladium tended to be closer to the SiC/OPyC interface suggests that palladium was primarily moving outward. The depletion of palladium in the SiC of Compact 2-3-2 particles after safety testing indicates that palladium was diffusing out faster than it was arriving at the IPyC/SiC interface. This was apparently not the case for uranium, which was building up both at the interface and in the SiC. The consistent presence of palladium in the IPyC/SiC interface region may be due to continued release of

palladium from the kernel or stabilization of palladium features at the interpenetrating regions of the IPyC/SiC interface (e.g., SiC "fingers"). Palladium release from the SiC is consistent with the observed uptick of palladium collecting on the CCCTF deposition cups after Compact 2-3-2 was at 1800°C for about 150 h (Figure 1). These observations of palladium and uranium transport at 1800°C are also corroborated by prior high temperature safety tests where the SiC layer was decorated by uranium-rich features and limited-palladium features were observed remaining in the SiC layer [Hunn et al. 2015b].

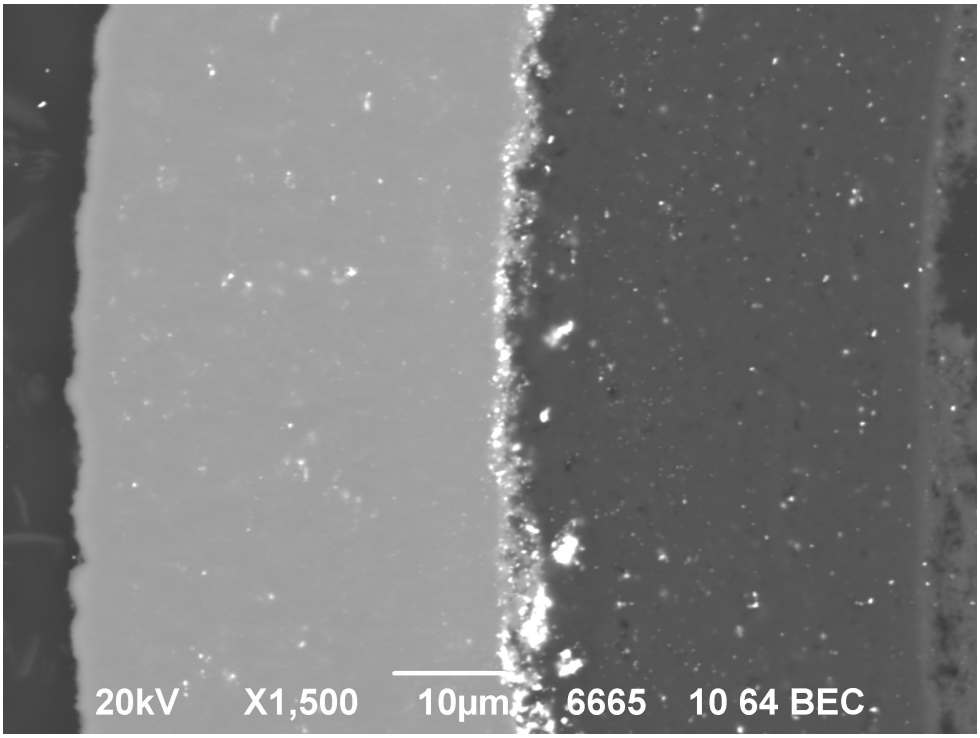

Figure 18. Electron micrograph of Particle 231-RS11 polished section showing (from left to right) OPyC, SiC with isolated high-Z features (fewer than in Figure 17), IPyC/SiC interface region with pileup of high-Z features, and IPyC with isolated high-Z features.

2.2 COMPACT 3-4-1 COMPARED TO COMPACT 3-4-2

2.2.1 Cesium and Krypton Release and Observed Particle Failure

Figure 19 shows the estimated 1700°C safety-test releases from AGR-2 UO_2 Compact 3-4-1 and Table 4 shows the distribution of fission products on the furnace internals at the end of the test. The cumulative fraction on the deposition cups at the end of the safety test (Table 4, Row 1) was used as an estimated collection efficiency for each individual cup to generate the time-dependent curves in Figure 19. The initial cesium release rate was very low but began to rise significantly during the Cup 4 residence period (i.e., after 13 h at 1700°C) and continued to rise at an ever-increasing rate throughout the remainder of the time at 1700°C. After 162 h at 1700°C the cumulative release of cesium was approaching 9% of the total inventory and the test, originally planned for 300 h at 1700°C, had to be prematurely terminated to prevent the dose rate of the furnace internals from rising above standard operating limits adhered to for hands-on maintenance of the furnace. The high cesium release fraction from Compact 3-4-1 at 1700°C indicates SiC failure in a large number of particles. A small but measurable amount of ^{85}Kr accumulated in the sweep gas trap in the latter half of the safety test (less than 7% of one particle's inventory), but levels were below what would be expected from failed TRISO and it is more likely that this ^{85}Kr was slowly diffusing through intact pyrocarbon from the large number of particles with failed SiC.

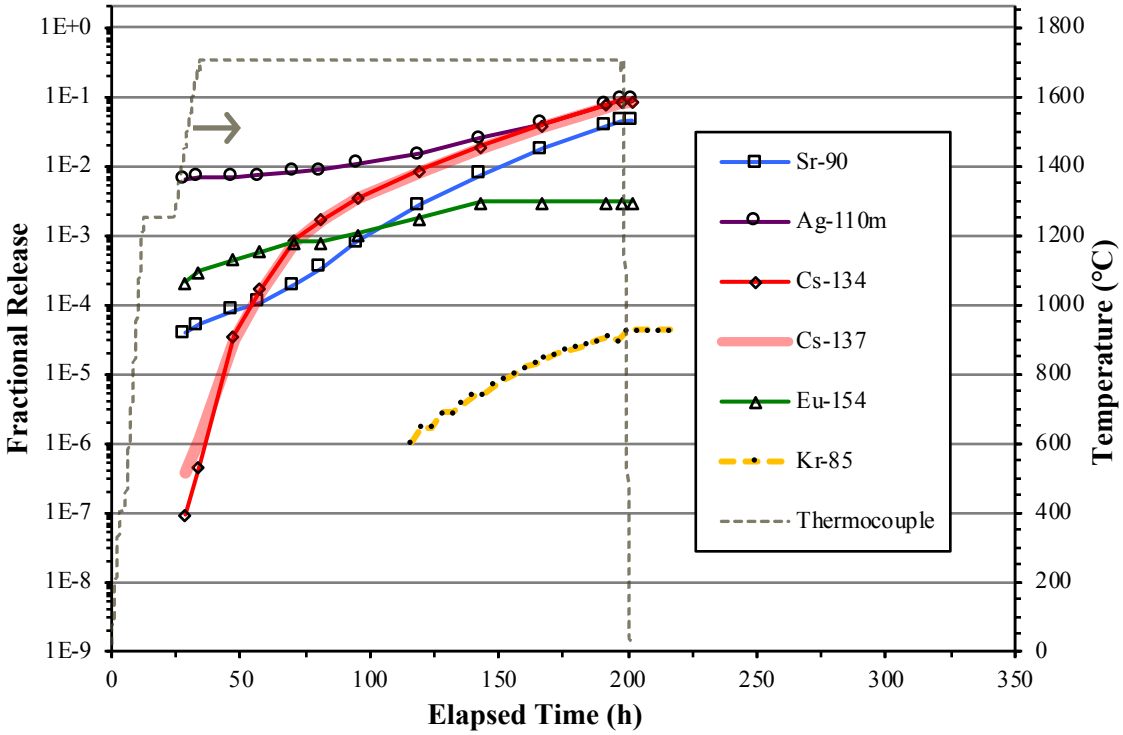

Figure 19. Release of fission products from Compact 3-4-1 during safety testing to 1700°C.

Table 4. Radioactive isotope distribution on furnace internal components after the Compact 3-4-1 safety test

Component	^{90}Sr	^{110m}Ag	^{134}Cs	^{137}Cs	^{154}Eu	^{155}Eu
Deposition cups	29.4%	100%	98.6%	98.4%	6.5%	8.2%
Tantalum parts	8.0%	~0%	0.81%	0.94%	15.8%	18.1%
Graphite holder	62.6%	~0%	0.60%	0.66%	77.7%	73.7%

Figure 20 shows the results of 110-second live-count-time gamma survey with the IMGA of all the particles recovered from Compact 3-4-1. This histogram provides evidence that numerous particles released some fraction of their ^{137}Cs. There were 150 particles with M/C ≤ 0.80 and it can be presumed with reasonable confidence that almost all these particles released some cesium. These particles were separated from the main population by the IMGA sorting process. However, the total estimated ^{137}Cs release from these 150 particles only accounts for roughly half of the ^{137}Cs measured on the CCCTF deposition cups and furnace internals. This means that there were numerous particles that released cesium with M/C > 0.80 that could not be separated out by the IMGA sorting process because their ^{137}Cs/^{144}Ce ratio was not distinct from the distribution of ^{137}Cs/^{144}Ce ratios for particles that did not release cesium. A rough accounting for the ^{137}Cs released in the CCCTF using the IMGA-measured amount of ^{137}Cs retained in the recovered Compact 3-4-1 particles and summing all particles starting from the left side of Figure 20 with the assumption that particles started with an average inventory of M/C = 1.05–1.10 yields an estimate of 400–800 particles with failed SiC (up to half of the particles in the compact). The exact number is somewhat irrelevant as the result is so far beyond a typical safety basis that use of an oxygen-gettered kernel design, such as UCO, for fuel intended for this level of burnup is clearly recommended by the safety test results if accident conditions might reach those tested.

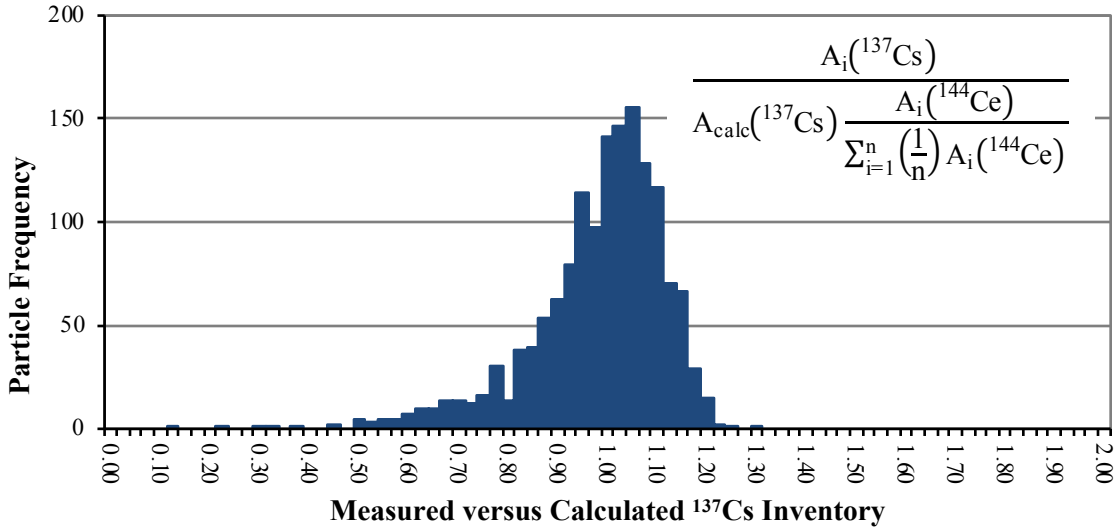

Figure 20. Ratio of ^{137}Cs retained in 1509 Compact 3-4-1 particles after safety testing to 1700°C versus the calculated inventory, adjusted for variation in fissionable material and burnup with the measured ^{144}Ce activity.

X-ray tomography of some of the particles with lower cesium retention has shown evidence for SiC failure similar to that reported for AGR-2 UO_2 Compacts 3-3-2 and 3-4-2 [Hunn et al. 2015a]. Namely, extensive CO corrosion of the SiC coupled with cracking of the SiC layer where it was weakened by the CO attack. The three particles shown in Figure 21 had the lowest cesium inventory of those surveyed with IMGA. Kernel material was missing from all three particles (more so from Particles 341-SP01 and 341-SP02). Cracks were evident in the buffer, IPyC, and SiC, but obvious cracks in the OPyC were not observed, while their presence is expected if the missing kernel material were due to leaching by acid infiltration during the deconsolidation and pre-burn leaching process. It is not known whether kernel material may have diffused out through intact OPyC during the 1700°C safety test or OPyC cracks were present that could not be resolved by the x-ray tomography. Extensive SiC corrosion was evident in these particles and localized where the SiC was exposed by IPyC fracture. Material appearing white in the x-ray images and deposited in open areas, such as gaps between buffer and IPyC and between buffer fragments, is presumably SiO_2 from the CO corrosion (based on observations of similar material in particles from Compacts 3-3-2 and 3-4-2). Cracks were observed that intersected and presumably started at the corrosion

spots. The three-dimensional (3D) visualization of Particle 341-SP03 in Figure 21 is an example and shows cracks extending out in three directions from the corrosion spot in the SiC. Further cross sectioning and analysis of some of these particles is planned.

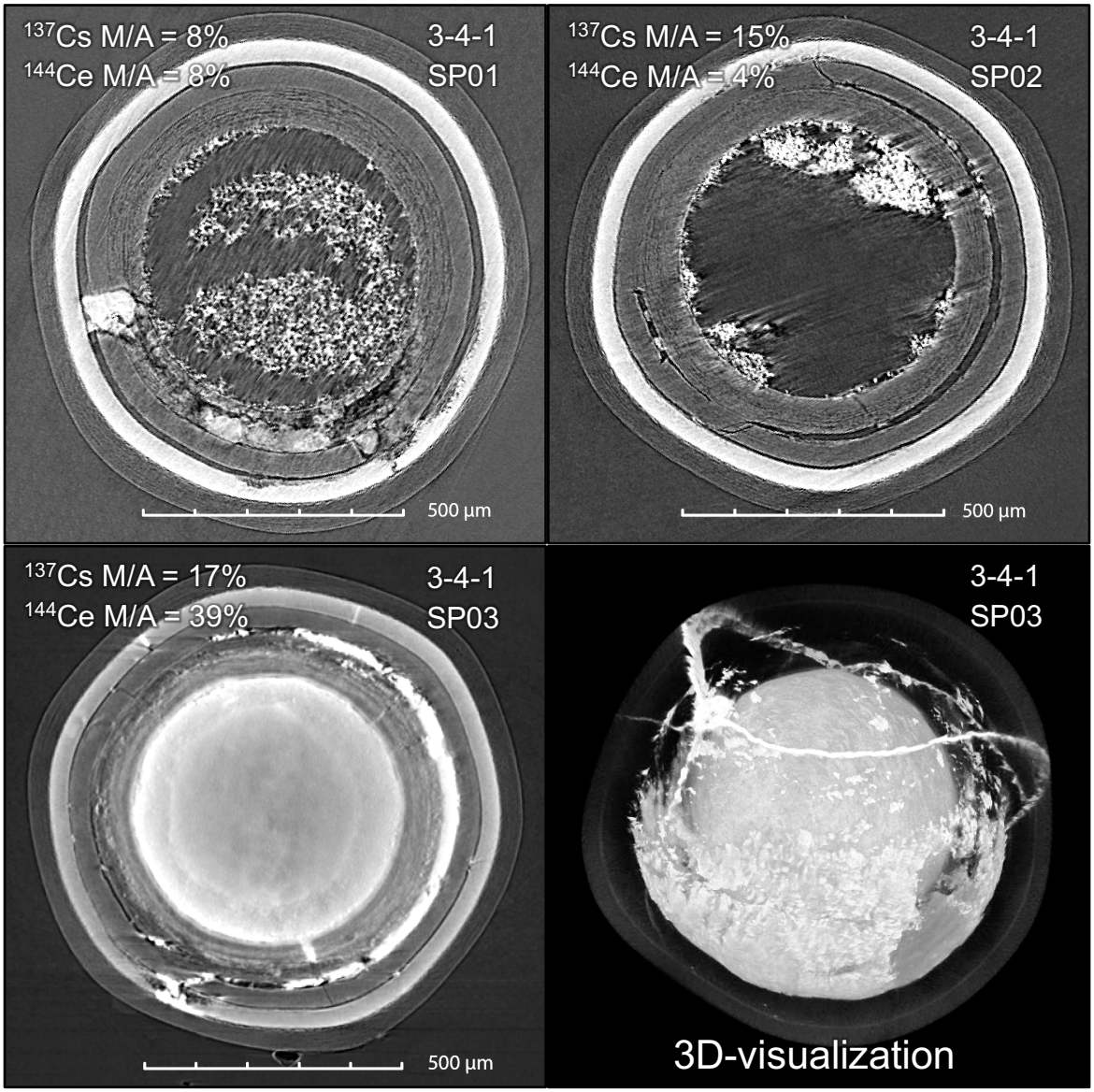

Figure 21. X-ray tomograms and a 3D-visualization of Compact 3-4-1 particles that released most of their cesium; the ^{137}Cs and ^{144}Ce fractional inventory is reported as measured/average (M/A).

Figure 22 shows four more particles that released cesium, but the retention in these particles was higher than those in Figure 21 and they had normal inventories of the other gamma-emitting isotopes measured by IMGA. Fracture of the IPyC was evident in all these particles. Figure 22 shows the IPyC fracture in Particles 341-SP04, 341-SP06, and 341-SP07 was located at the boundary between detached and bonded buffer, which has been found to be a common mode of IPyC fracture (the other being propagation of a buffer crack into IPyC still bonded to the buffer when the crack reaches the buffer/IPyC interface) [Hunn et al. 2014a]. These particles did not exhibit the advanced localized corrosion seen in the particles with lower cesium retention, but there was general corrosion at the IPyC/SiC interface. This corrosion was most pronounced in Particle 341-SP05, which also showed what was presumably SiO_2 in the buffer/IPyC

gap. The tomogram of Particle 341-SP07 also shows a fine-line crack in the SiC. A similar crack was found in Particle 341-SP04, but cracks could not be resolved in the other two particles.

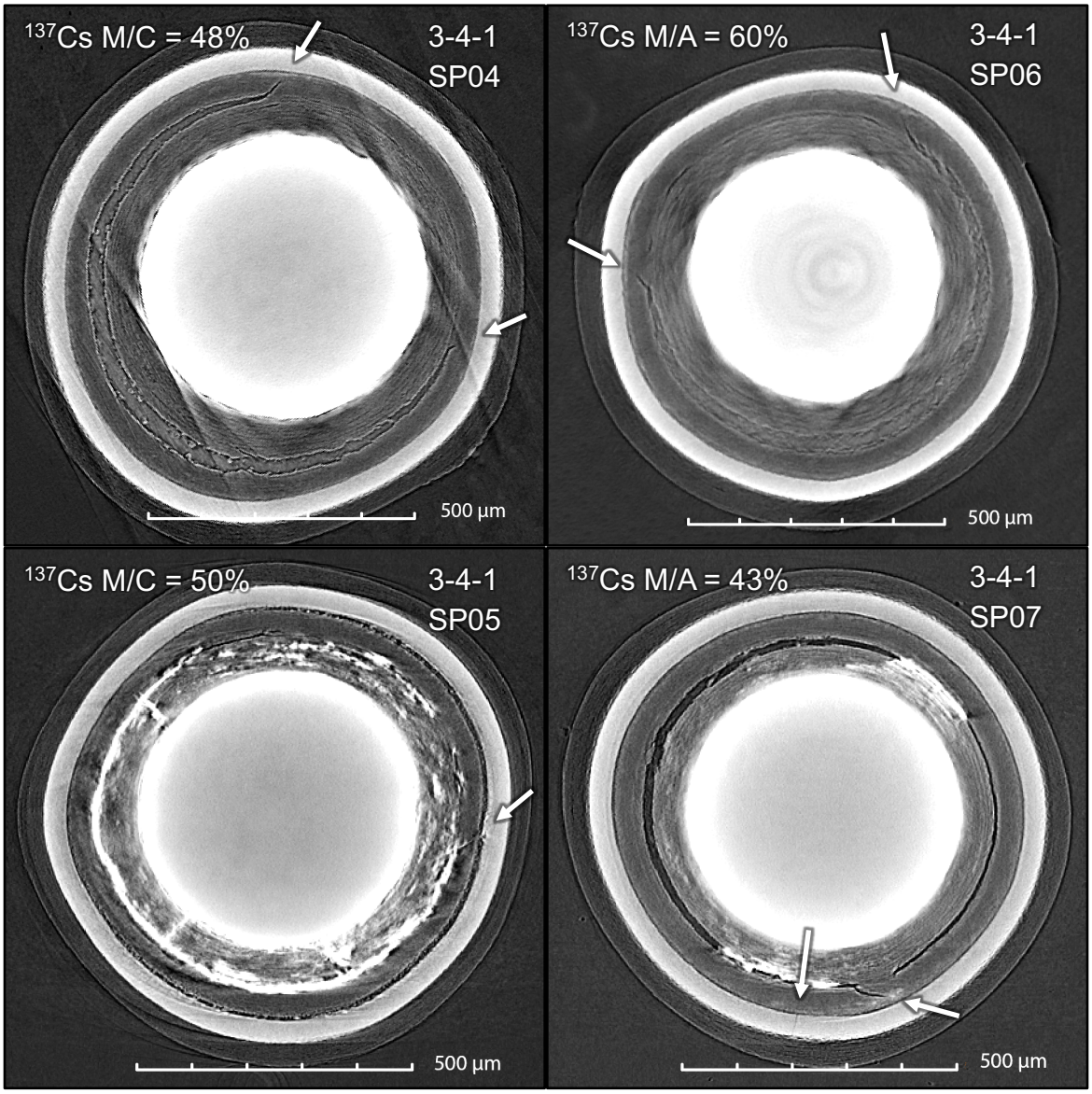

Figure 22. X-ray tomograms of Compact 3-4-1 particles that released cesium; the ^{137}Cs fractional inventory is reported as M/C and cracks are marked with arrows.

2.2.2 Silver Release

Silver-110m release over the first 50 h of the Compact 3-4-1 safety test at 1700°C (Figure 19) was similar to what was observed during 1600°C safety testing of its twin, AGR-2 UO_2 Compacts 3-4-2 (Figure 23) and typical of all AGR safety tests as a result of silver released from the matrix and/or OPyC. Figure 24 and Figure 25 show the estimated average release rate during each deposition cup residence period from Compact 3-4-1 and Compacts 3-4-2, respectively. In both cases, the ^{110m}Ag release rate dropped after the initial release from the matrix and/or OPyC then increased as particle failure occurred, closely matching the ^{134}Cs and ^{137}Cs release rates. This indicates that the silver release was dominated by the same SiC failure that was causing the cesium release.

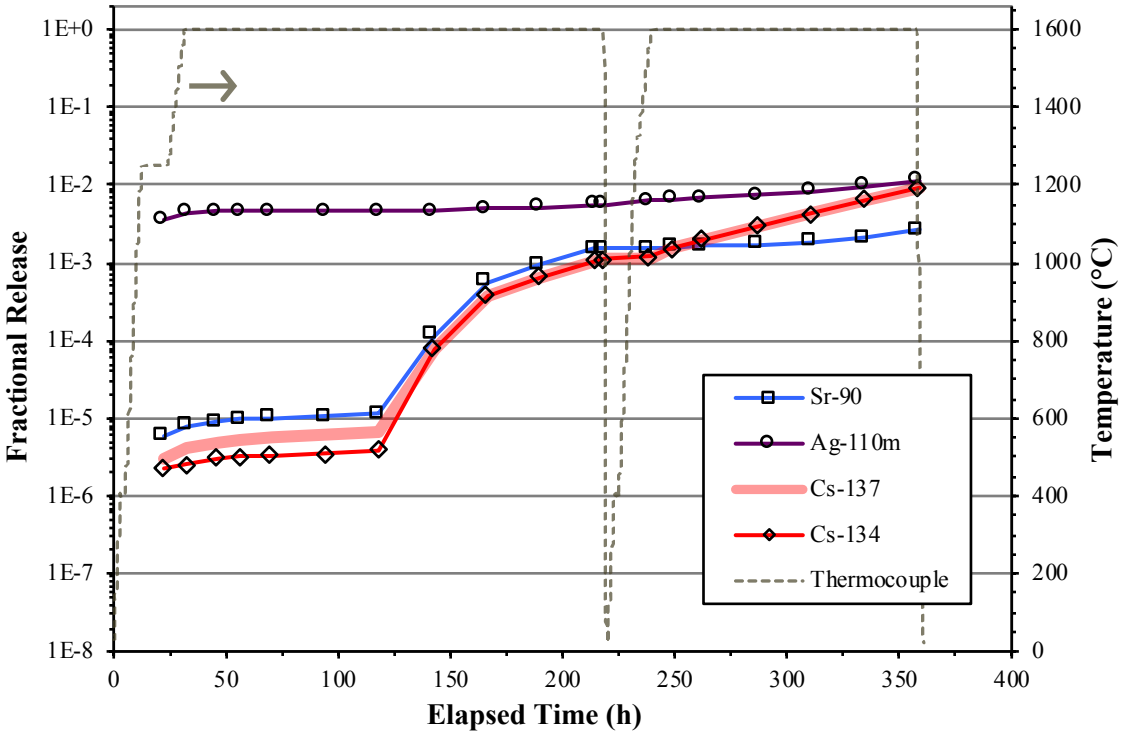

Figure 23. Release of fission products from Compact 3-4-2 during safety testing to 1600°C (the interruption in the temperature after 187 h at 1600°C was due to a blockage in a cooling water line) [Hunn et al. 2015a].

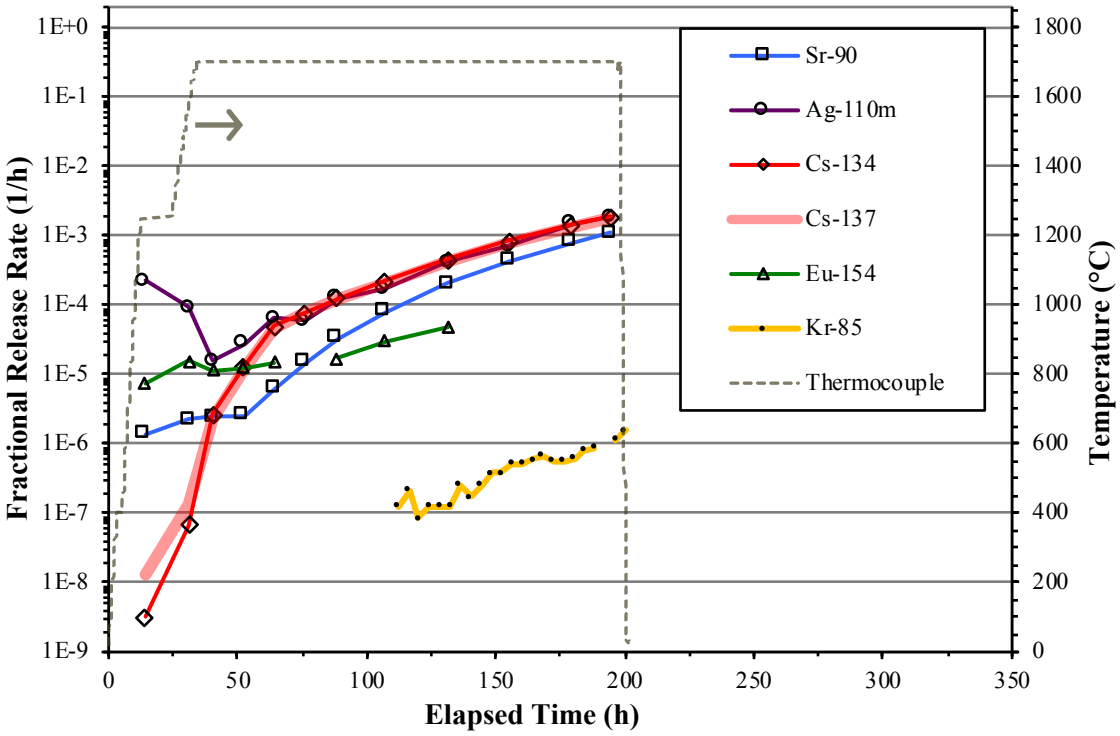

Figure 24. Rate of fission product release from Compact 3-4-1 during safety testing to 1700°C.

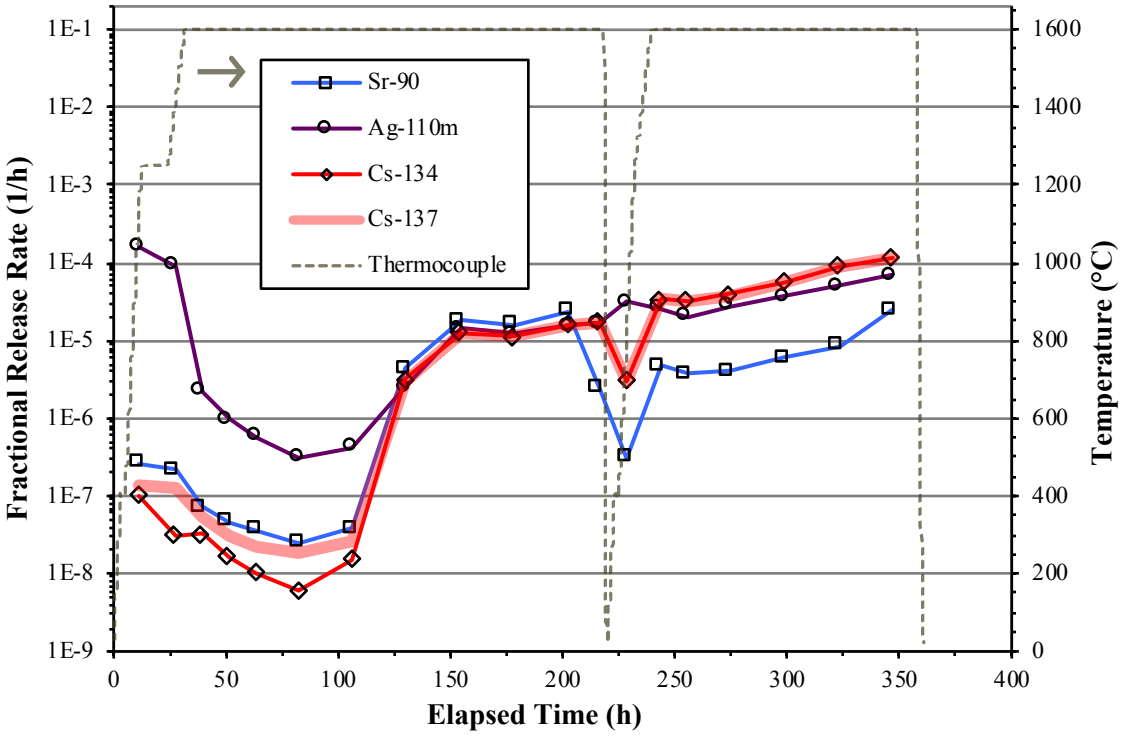

Figure 25. Rate of fission product release from Compact 3-4-2 during safety testing to 1600°C.

2.2.3 Strontium and Europium Release

Figure 24 and Figure 25 show that the fractional release rate of ^{90}Sr, like ^{110m}Ag, was dominated by the SiC failure as the Compact 3-4-1 and 3-4-2 safety tests progressed. It is likely that the lagging behavior, compared to silver and cesium, is a result of a slower diffusion of strontium out of particles with failed SiC and the already discussed holdup that would occur in the matrix graphite and surrounding graphite holder. There could also be some impact from a higher stability of strontium in the UO_2 kernel, where it is expected to reside as an oxide [McMurray et al. 2017].

The available data makes it look like europium release behavior from Compact 3-4-1 at 1700°C was different from strontium (Figure 19). This is consistent with results from 1600°C safety testing of AGR-2 UO_2 Compacts 3-3-2 and 3-4-2 [Hunn et al. 2015a] and may be related to europium's stability in the UO_2 kernel. However, the very high activities of ^{134}Cs and ^{137}Cs on the deposition cups and the counting conditions required for the higher-activity cups made it difficult to get reliable measurement of the europium isotopes released in the latter half of the Compact 3-4-1 test. Therefore, the accuracy of the europium release data is suspect. Strontium was not impacted in this way because the beta emission from ^{90}Sr was measured after isotopic separation from the gamma emitting isotopes. Also impacting the interpretation of the strontium and europium results is the fact that most of these isotopes were found in the graphite holder at the end of the test and this impacts the accuracy of the estimation of the cup collection efficiency.

3. CONCLUSION

Safety testing was completed at 1800°C on AGR-2 UCO Compact 2-3-2 and at 1700°C on AGR-2 UO_2 Compact 3-4-1. The UO_2 compact was not tested at 1800°C because of concerns from results at 1600°C that indicated that multiple particle failures from CO corrosion were probable [Hunn et al. 2015a]. These concerns were warranted and 1800°C safety testing of AGR-2 UO_2 fuel is not recommended.

The AGR-2 UCO Compact 2-3-2 safety test performance and fission product release was compared to two previous AGR-2 UCO compact safety tests: a 1600°C safety testing of its twin (AGR-2 UCO Compact 2-3-1) and an 1800°C safety testing of AGR-2 UCO Compact 5-4-1, which was irradiated at a lower temperature (Table 1). The AGR-2 UO_2 Compact 3-4-1 safety test performance and fission product release was compared to its 1600°C safety-tested twin: AGR-2 UO_2 Compact 3-4-2. Table 5 is a summary of the cumulative release from the safety tests of these compacts.

Table 5. Cumulative releases of radioactive isotopes from compacts discussed in this report

	Compact 2-3-2	Compact 2-3-1	Compact 5-4-1	Compact 3-4-1	Compact 3-4-2
	1800°C	1600°C	1800°C	1700°C	1600°C
^{85}Kr	4.03×10^{-4} (1.28)	$<7\times10^{-7}$ (<0.002)	$<7\times10^{-7}$ (<0.002)	4.33×10^{-5} (0.067)	$<1\times10^{-6}$ (<0.002)
^{90}Sr	9.85×10^{-2} (313)	8.61×10^{-2} (273)	2.34×10^{-3} (7.43)	4.47×10^{-2} (68.9)	2.70×10^{-3} (4.16)
^{110m}Ag	2.48×10^{-2} (78.7)	1.76×10^{-2} (55.8)	1.73×10^{-1} (550)	8.92×10^{-2} (138)	1.13×10^{-2} (17.5)
^{134}Cs	2.95×10^{-4} (0.94)	3.96×10^{-6} (0.013)	1.03×10^{-4} (0.33)	8.72×10^{-2} (135)	9.29×10^{-3} (14.3)
^{137}Cs	3.35×10^{-4} (1.06)	-	1.18×10^{-4} (0.37)	8.21×10^{-2} (127)	9.21×10^{-3} (14.2)
^{154}Eu	1.35×10^{-1} (429)	8.77×10^{-2} (278)	6.04×10^{-3} (19.2)	3.05×10^{-3} (4.70)	3.15×10^{-4} (0.49)
^{155}Eu	1.31×10^{-1} (416)	8.36×10^{-2} (265)	5.72×10^{-3} (18.2)	4.14×10^{-3} (6.38)	3.67×10^{-4} (0.57)

Values are reported as compact fractions and particle-equivalents (in parentheses).

Krypton release at the beginning of the Compact 2-3-2 safety test, in conjunction with cesium release, indicated that there was a particle with TRISO failure either prior to the start of the safety test or the failure occurred as the compact was raised to 1800°C. The compact was deconsolidated, and particles were scanned with the IMGA. One particle was found, and x-ray tomography showed massive localized degradation of the SiC layer. Subsequent SEM/EDS analysis revealed the failure to be related to reaction with molybdenum, which may have come from outside the particle given the appearance of the degraded region and the fact that molybdenum inclusions were observed in an as-fabricated AGR-2 fuel particle. The observed leaching of exposed kernels and presumed coating failure during DLBL of Compact 2-3-2 introduces some uncertainty in the number of particles that experienced coating failure during the safety test, but the one failed-TRISO particle that was recovered had very little cesium remaining and could account for the observed cesium and krypton releases during safety testing.

A small amount of ^{85}Kr release during Compact 3-4-1 safety testing was too low to have come from a particle with failed TRISO and probably came from diffusion of krypton through intact OPyC of particles with failed SiC. SiC failure, as indicated by the cesium release at 1700°C involved 400–800 particles, based on balancing the cesium release in the CCCTF against the inventory in each particle measured with the IMGA.

Silver release was high from all compacts. Compact twins AGR-2 UCO Compact 2-3-2 and AGR-2 UCO Compact 2-3-1 had similar silver release that was mostly related to silver retained in the matrix and/or OPyC from earlier release during irradiation. The silver from AGR-2 UCO Compact 5-4-1 was much higher and dominated by release through intact SiC during the 1800°C safety test. Compact 2-3-2 particles also released silver through intact SiC, but the effect was less dramatic due to a lower internal silver inventory at the start of the test. The silver release from the UO_2 compacts was dominated by release from particle with SiC failure.

Europium and strontium releases from AGR-2 UCO Compacts 2-3-2 and 2-3-1 were higher than the other compacts because of high releases during the higher temperature irradiation and good retention in the matrix and OPyC until the compacts were heated to safety test temperatures. This is consistent with previous studies of other Capsule 2 compacts [Hunn et al. 2016b].

4. REFERENCES

Baldwin, C.A., J.D. Hunn, R.N. Morris, F.C. Montgomery, C.M. Silva, and P.A. Demkowicz. 2012. "First Elevated Temperature Performance Testing of Coated Particle Fuel Compacts from the AGR-1 Irradiation Experiment." Paper HTR2012-3-027. *Proc. 6th International Topical Meeting on High Temperature Reactor Technology (HTR-2012)*, Tokyo, Japan, October 28–November 1, 2012. Also published in *Nucl. Eng. and Design* 271: 131–141.

Barnes, C.M. and D.W. Marshall. 2009. *FY 2009 Particle Fabrication and Coater Test Report.* INL/EXT-09-16545, Revision 0. Idaho Falls, ID: Idaho National Laboratory.

Collin, B.P. 2014. *AGR-2 Irradiation Test Final As-Run Report.* INL/EXT-14-32277, Revision 2. Idaho Falls, ID: Idaho National Laboratory.

Demkowicz, P.A. 2013. *AGR-2 Post Irradiation Examination Plan.* PLN-4616, Revision 0. Idaho Falls, ID: Idaho National Laboratory.

Demkowicz, P.A., J.D. Hunn, R.N. Morris, I.J. van Rooyen, T.J. Gerczak, J.M. Harp, and S.A. Ploger. 2015. *AGR-1 Post Irradiation Examination Final Report.* INL/EXT-15-36407, Revision 0. Idaho Falls, ID: Idaho National Laboratory.

Gerczak, T.J., J.D. Hunn, R.A. Lowden, and T.R. Allen. 2016. "SiC Layer Microstructure in AGR-1 and AGR-2 TRISO Fuel Particles and the Influence of Its Variation on the Effective Diffusion of Key Fission Products." *J. Nucl. Mater.* 480: 1–14.

Harp, J.M., P.A. Demkowicz, and J.D. Stempien. 2016. "Fission Product Inventory and Burnup Evaluation of the AGR-2 Irradiation by Gamma Spectrometry", Paper HTR2016-18593. *Proc. 8th International Topical Meeting on High Temperature Reactor Technology (HTR-2016)*, Las Vegas, Nevada, November 6–10, 2016. Also published in *Nucl. Eng. and Design* 329: 134–141.

Hawkes, G.L. 2014. *AGR-2 Daily As-Run Thermal Analyses.* INL/ECAR-2476, Revision 1. Idaho Falls, ID: Idaho National Laboratory.

Hunn, J.D. and R.A. Lowden. 2006. *Data Compilation for AGR-1 Variant 3 Coated Particle Composite LEU01-49T.* ORNL/TM-2006/022, Revision 0. Oak Ridge, TN: Oak Ridge National Laboratory.

Hunn, J.D. 2009. *Data Compilation for AGR-2 B&W UO_2 Coated Particle Batch G73H-10-93085B*. ORNL/TM-2009/255, Revision 1. Oak Ridge, TN: Oak Ridge National Laboratory.

Hunn, J.D. 2010. *AGR-2 Fuel Compacts Information Summary: Prepared for the NRC MELCOR Project*. ORNL/TM-2010/296, Revision 1. Oak Ridge, TN: Oak Ridge National Laboratory.

Hunn, J.D., F.C. Montgomery, and P.J. Pappano. 2010a. *Data Compilation for AGR-2 UCO Variant Compact Lot LEU09-OP2-Z.* ORNL/TM-2010/017, Revision 1. Oak Ridge, TN: Oak Ridge National Laboratory.

Hunn, J.D., F.C. Montgomery, and P.J. Pappano. 2010b. *Data Compilation for AGR-2 UO_2 Compact Lot LEU11-OP2-Z.* ORNL/TM-2010/055, Revision 1. Oak Ridge, TN: Oak Ridge National Laboratory.

Hunn, J.D., T.W. Savage, and C.M. Silva. 2010. *AGR-2 Fuel Compact Pre-Irradiation Characterization Summary Report.* ORNL/TM-2010/226, Revision 0. Oak Ridge, TN: Oak Ridge National Laboratory.

Hunn, J.D., T.W. Savage, and C.M. Silva. 2012. *AGR-1 Fuel Compact Pre-Irradiation Characterization Summary Report.* ORNL/TM-2012/295, Revision 0. Oak Ridge, TN: Oak Ridge National Laboratory.

Hunn, J.D., R.N. Morris, C.A. Baldwin, F.C. Montgomery, C.M. Silva, and T.J. Gerczak. 2013, *AGR-1 Irradiated Compact 4-4-2 PIE Report: Evaluation of As-Irradiated Fuel Performance with Leach Burn Leach, IMGA, Materialography, and X-ray Tomography*. ORNL/TM-2013/236, Revision 0. Oak Ridge, TN: Oak Ridge National Laboratory.

Hunn, J.D., C.A. Baldwin, T J. Gerczak, F.C. Montgomery, R.N. Morris, C.M. Silva, P.A. Demkowicz, J.M. Harp, S.A. Ploger, I.J. van Rooyen, and K.E. Wright. 2014a. "Detection and Analysis of Particles with Failed SiC in AGR-1 Fuel Compacts." Paper HTR2014-31254. *Proc. 7th International Topical Meeting on High Temperature Reactor Technology (HTR-2014)*, Weihai, China, October 27–31, 2014. Also published in *Nucl. Eng. Design* 360: 36–46.

Hunn, J.D., R.N. Morris, C.A. Baldwin, F.C. Montgomery, and T.J. Gerczak. 2014b, *PIE on Safety-Tested AGR-1 Compacts 5-3-3, 5-1-3, and 3-2-3*. ORNL/TM-2014/484, Revision 0. Oak Ridge, TN: Oak Ridge National Laboratory.

Hunn, J.D., R.N. Morris, C.A. Baldwin, and F.C. Montgomery. 2015a. *Safety-Testing of AGR-2 UO_2 Compacts 3-3-2 and 3-4-2*. ORNL/TM-2015/388, Revision 0. Oak Ridge, TN: Oak Ridge National Laboratory.

Hunn, J.D., T.J. Gerczak , R.N. Morris, C.A. Baldwin, and F.C. Montgomery. 2015b. *PIE on Safety-Tested Loose Particles from AGR-1 Compact 4-2-2*. ORNL/TM-2015/161, Revision 0. Oak Ridge, TN: Oak Ridge National Laboratory.

Hunn, J.D., R.N. Morris, C.A. Baldwin, and F.C. Montgomery. 2016a. *Safety-Testing of AGR-2 UCO Compacts 5-2-2, 2-2-2, and 5-4-1*. ORNL/TM-2016/423, Revision 1. Oak Ridge, TN: Oak Ridge National Laboratory.

Hunn, J.D., C.A. Baldwin, F.C. Montgomery, T.J. Gerczak, R.N. Morris, G.W. Helmreich, P.A. Demkowicz, J.M. Harp, and J.D. Stempien. 2016b. "Initial Examination of Fuel Compacts and TRISO Particles from the US AGR-2 Irradiation Test." Paper HTR2016-18443. *Proc. 8th International Topical Meeting on High Temperature Reactor Technology (HTR-2016)*, Las Vegas, Nevada, November 6–10, 2016. Also published in *Nucl. Eng. Design* 329: 89–101.

Hunn, J.D., T.J. Gerczak, R.N. Morris, C.A. Baldwin, and F.C. Montgomery. 2016c. PIE on *Safety-Tested Loose Particles from AGR-1 Compact 4-4-2*. ORNL/TM-2015/161, Revision 0. Oak Ridge, TN: Oak Ridge National Laboratory.

Hunn, J.D., R.N. Morris, C.A. Baldwin, Z.M. Burns, F.C. Montgomery, and D.J. Skitt. 2017. *Safety-Testing of AGR-2 UCO Compacts 6-4-2 and 2-3-1*. ORNL/TM-2017/439, Revision 0. Oak Ridge, TN: Oak Ridge National Laboratory.

Hunn, J.D., R.N. Morris, F.C. Montgomery, T.J. Gerczak, D.J. Skitt, C.A. Baldwin, J.A. Dyer, G.W. Helmreich, B.D. Eckhart, Z.M. Burns, P.A. Demkowicz, and J.D. Stempien. 2018. "Post-Irradiation Examination and Safety Testing of US AGR-2 Irradiation Test Compacts." Paper HTR2018-0010. *Proc. 9th International Topical Meeting on High Temperature Reactor Technology (HTR-2018)*, Warsaw, Poland, October 8–10, 2018.

Lowden, R.A. 2006. *Fabrication of Baseline and Variant Particle Fuel for AGR-1*. ORNL/CF-2006/02, Revision 0. Oak Ridge, TN: Oak Ridge National Laboratory.

McMurray, J.W., T.B. Lindemer, N.R. Brown, T.J. Reif, R.N. Morris, and J.D. Hunn. 2017. "Determining the Minimum Required Uranium Carbide Content for HTGR UCO Fuel Kernels." *Annals of Nuclear Energy* **104** (2017) 237–242.

Morris, R.N., P.A. Demkowicz, J.D. Hunn, C.A. Baldwin, and E.L. Reber. 2014. "Performance of AGR-1 High Temperature Reactor Fuel During Post-Irradiation Heating Tests." Paper HTR2014-31135 in *Proceedings of the HTR 2014,* Weihai, China, October 27–31, 2014. Also published in *Nucl. Eng. Design* 306: 24–35.

Morris, R.N., J.D. Hunn, C.A. Baldwin, F.C. Montgomery, T.J. Gerczak, and P.A. Demkowicz. 2016. "Initial Results from Safety Testing of US AGR-2 Irradiation Test Fuel." Paper HTR2016-18574. *Proc. 8th International Topical Meeting on High Temperature Reactor Technology (HTR-2016)*, Las Vegas, Nevada, November 6–10, 2016. Also published in *Nucl. Eng. Design* 329: 124–133.

Phillips, J.A., C.M. Barnes, and J.D. Hunn. 2010. "Fabrication and Comparison of Fuels for Advanced Gas Reactor Irradiation Tests." Paper HTR2010-236. *Proc. 5th International Topical Meeting on High Temperature Reactor Technology (HTR-2010)*, Prague, Czech Republic, October 18–20, 2010.

Sterbentz, J.W. 2014. *JMOCUP As-Run Daily Depletion Calculation for the AGR-2 Experiment in the ATR B-12 Position.* ECAR-2066, Revision 2. Idaho Falls, ID: Idaho National Laboratory.

Wilhelm, H.A. 1964. *The Carbon Reduction of Uranium Oxide.* USAEC/IS-1023, Revision 0. Ames, Iowa: Ames Laboratory at Iowa State University of Science and Technology.